Supporting Information

Exploring Pyrazolidinone and Pyrazolidinedione Scaffolds for Alzheimer's Therapy: Multitarget COX-2 Inhibitors with Anti-Amyloid β, Anti-Tau, Antioxidant, and Neuroprotective Activities

AUTHOR NAMES

Michael Emad[1#], Reham Waheed[1#], Zeinab Mostafa[1], Sarah S. Darwish[1,2], Rosa Purgatorio[3], Daniela Valeria Miniero[4], Annalisa De Palma[5], Tzu-Peng Cheng[6], Moustafa Gabr[7], Ahmed M. El Kerdawy[8,9], Marco Catto[3], Ashraf H. Abadi[1], Tsong-Long Hwang[6,10-13]* and Mohammad Abdel-Halim[1]**

AUTHOR ADDRESS

[1]Department of Pharmaceutical Chemistry, Faculty of Pharmacy and Biotechnology, German University in Cairo, Cairo 11835, Egypt.

[2]School of Life and Medical Sciences, University of Hertfordshire hosted by Global Academic Foundation, New Administrative Capital, 11578 Cairo, Egypt

[3]Department of Pharmacy and Pharmaceutical Sciences, University of Bari Aldo Moro, via E. Orabona 4, 70125 Bari (Italy).

[4]Department of Medicine and Surgery, LUM University Giuseppe Degennaro, Torre Rossi, 70010 Casamassima (Italy)

[5]Department of Biosciences, Biotechnologies and Environment, University of Bari Aldo Moro, via E. Orabona 4, 70125 Bari (Italy)

[6]Graduate Institute of Natural Products, College of Medicine, Chang Gung University, Taoyuan 333, Taiwan

[7]Department of Radiology, Molecular Imaging Innovations Institute (MI3), Weill Cornell Medicine, New York, NY 10065, USA

[8]School of Health and Care Sciences, College of Health and Science, University of Lincoln, Joseph Banks Laboratories, Green Lane, Lincoln, United Kingdom.

[9]Department of Pharmaceutical Chemistry, Faculty of Pharmacy, Cairo University, Kasr El-Aini Street, P.O. Box 11562, Cairo, Egypt.

[10]Center for Drug Research and Development, Graduate Institute of Health Industry Technology, College of Human Ecology, Chang Gung University of Science and Technology, Taoyuan 333, Taiwan

[11]Department of Anesthesiology, Chang Gung Memorial Hospital, Taoyuan 333, Taiwan

[12]School of Chinese Medicine, College of Medicine, National Yang Ming Chiao Tung University, Taipei 112, Taiwan

[13]Department of Chemical Engineering, Ming Chi University of Technology, New Taipei City 243, Taiwan

# Authors equally contributed to this work.

* To whom correspondence should be addressed:

Tsong-Long Hwang (htl@mail.cgust.edu.tw) and Mohammad Abdel-Halim (Mohammad.abdel-halim@guc.edu.eg)

Content

1. Figure S1

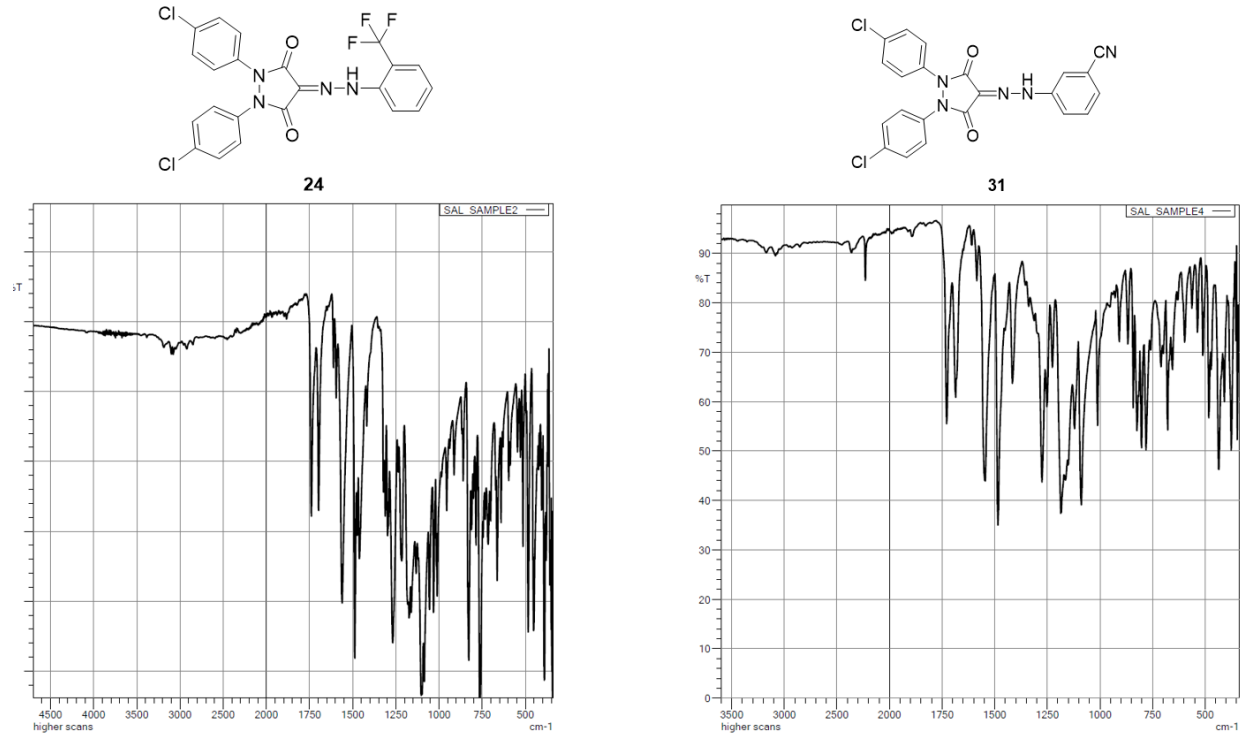

Figure S1: IR charts of compounds 24 and 31

2. Figure S2

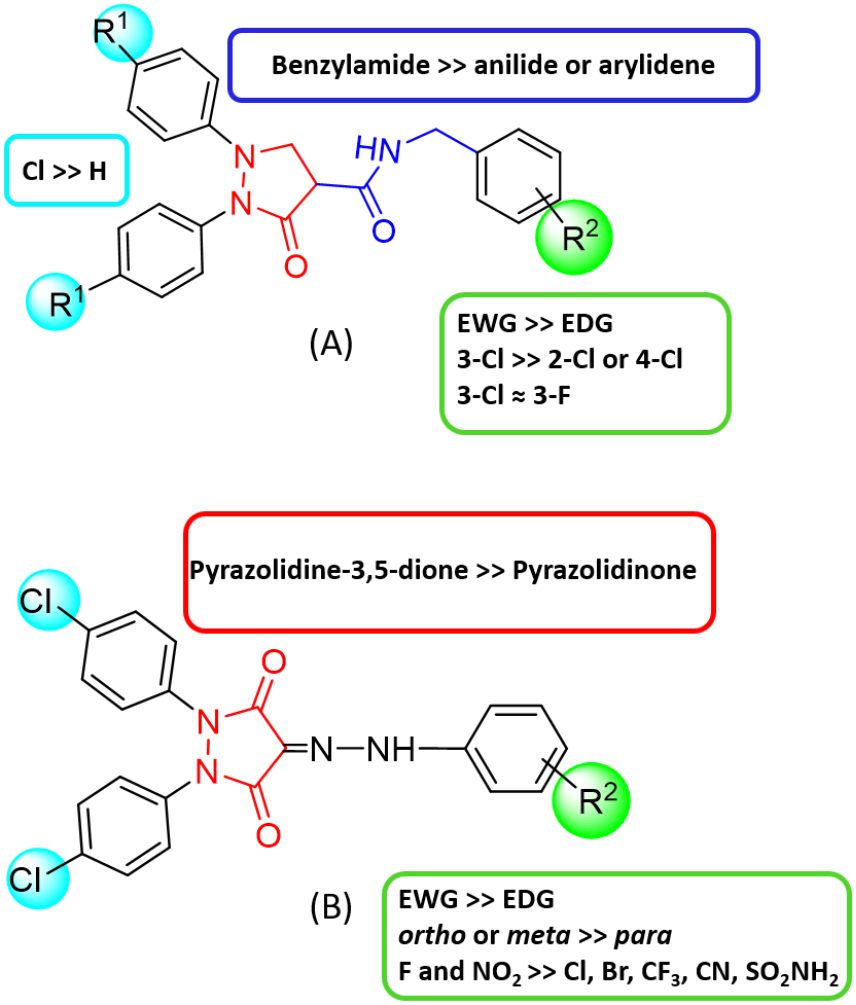

Figure S2: (A) First series SAR summary. (B) Second series SAR summary.

3. ^{1}H NMR and ^{13}C NMR spectra of representative compounds

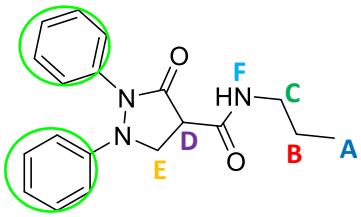

(2)

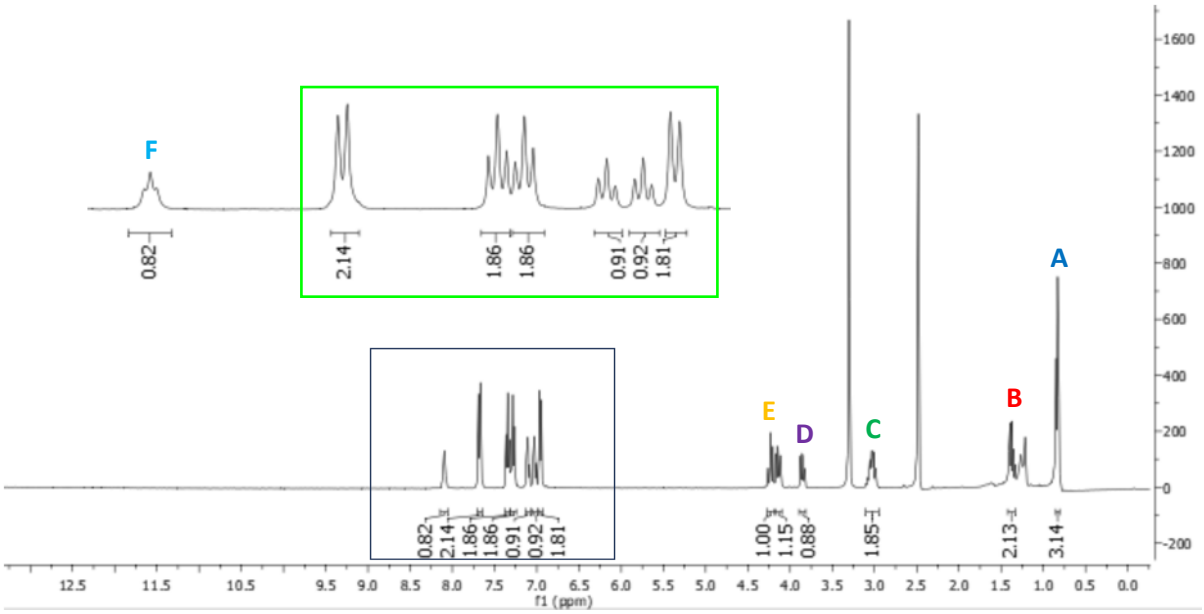

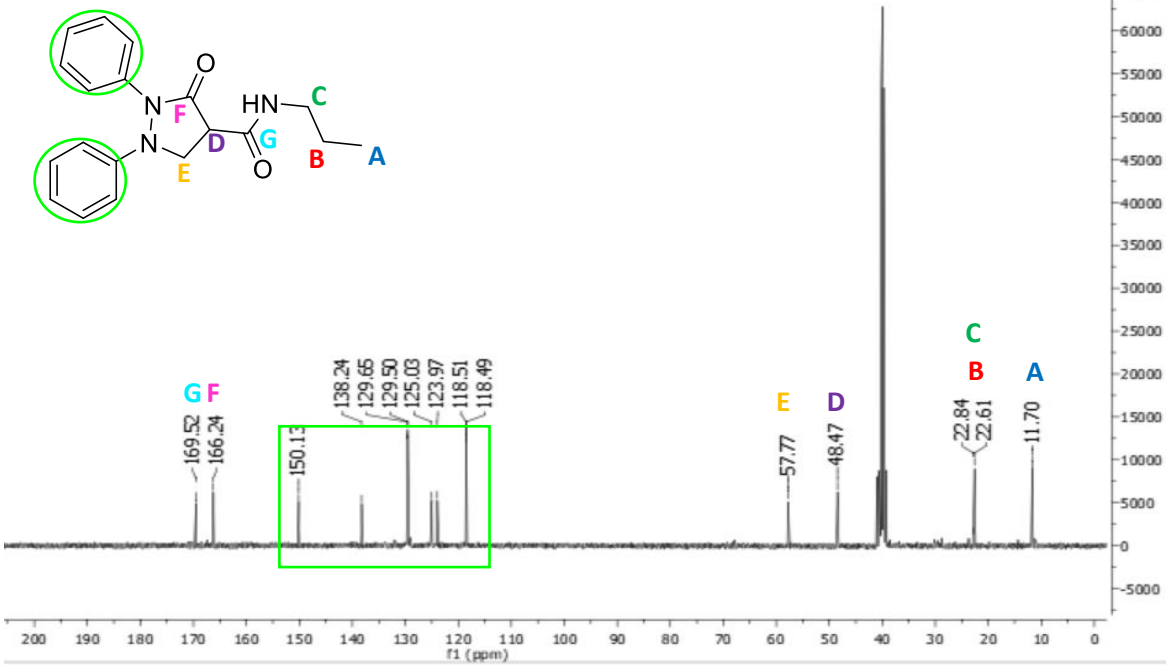

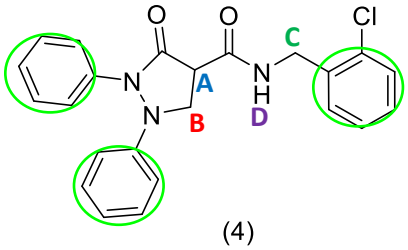
O
O
Cl
C
N
A
N
H
B
D

(4)

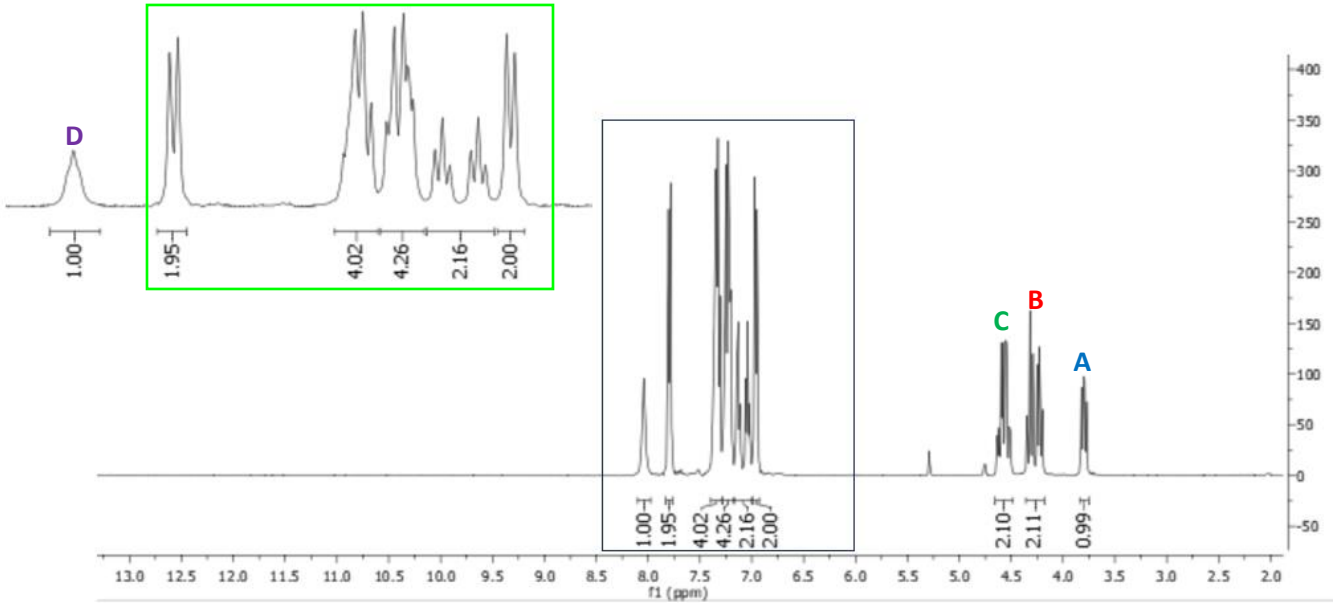
D
1.00
1.95
4.02
4.26
2.16
2.00
C
B
A
2.10
2.11
0.99
f1 (ppm)

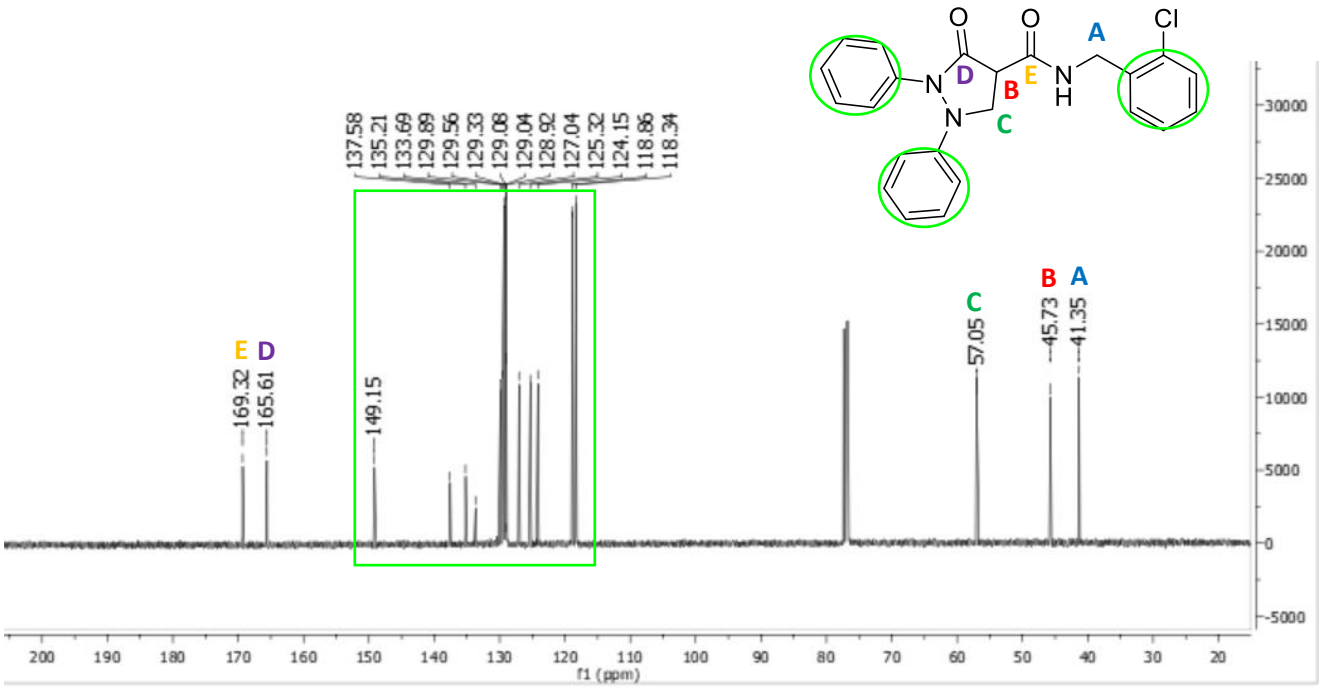
O
O
A
Cl
N
D
B
E
N
H
C
137.58
135.21
133.69
129.89
129.56
129.33
129.08
129.04
128.92
127.04
125.32
124.15
118.86
118.34
E
D
169.32
165.61
149.15
C
57.05
B
A
45.73
41.35
f1 (ppm)

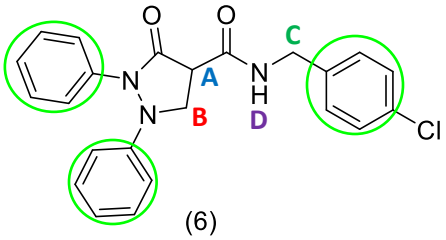
O
O
C
A
N
H
N
B
D
Cl

(6)

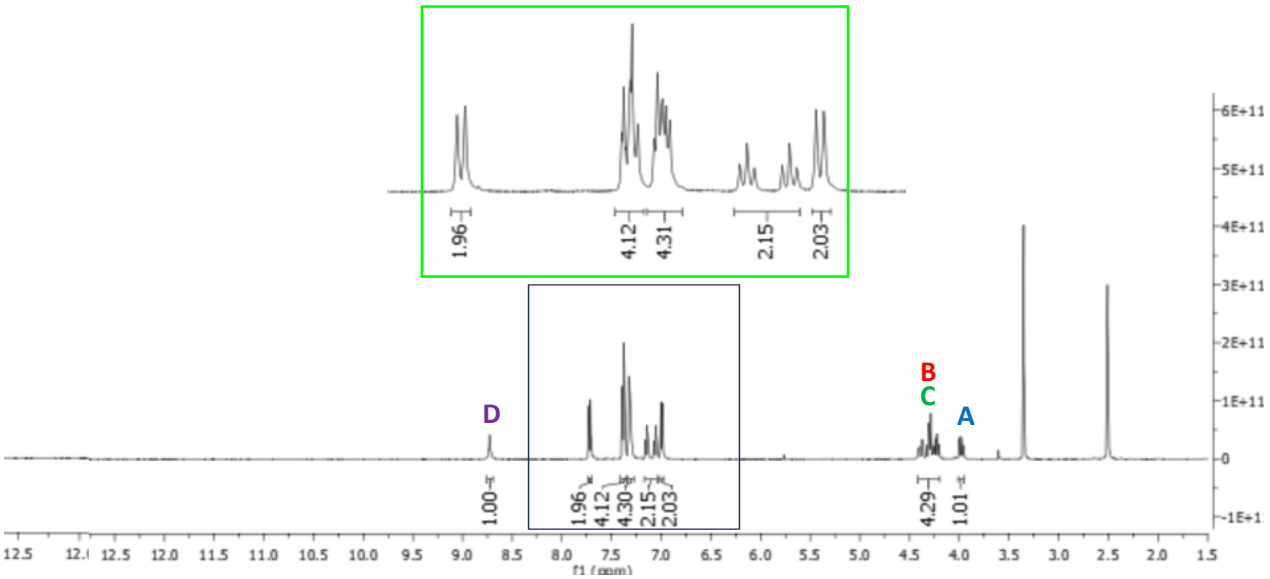
1.96
4.12
4.31
2.15
2.03
D
B
C
A
1.00
1.96
4.12
4.30
2.15
2.03
4.29
1.01
f1 (ppm)

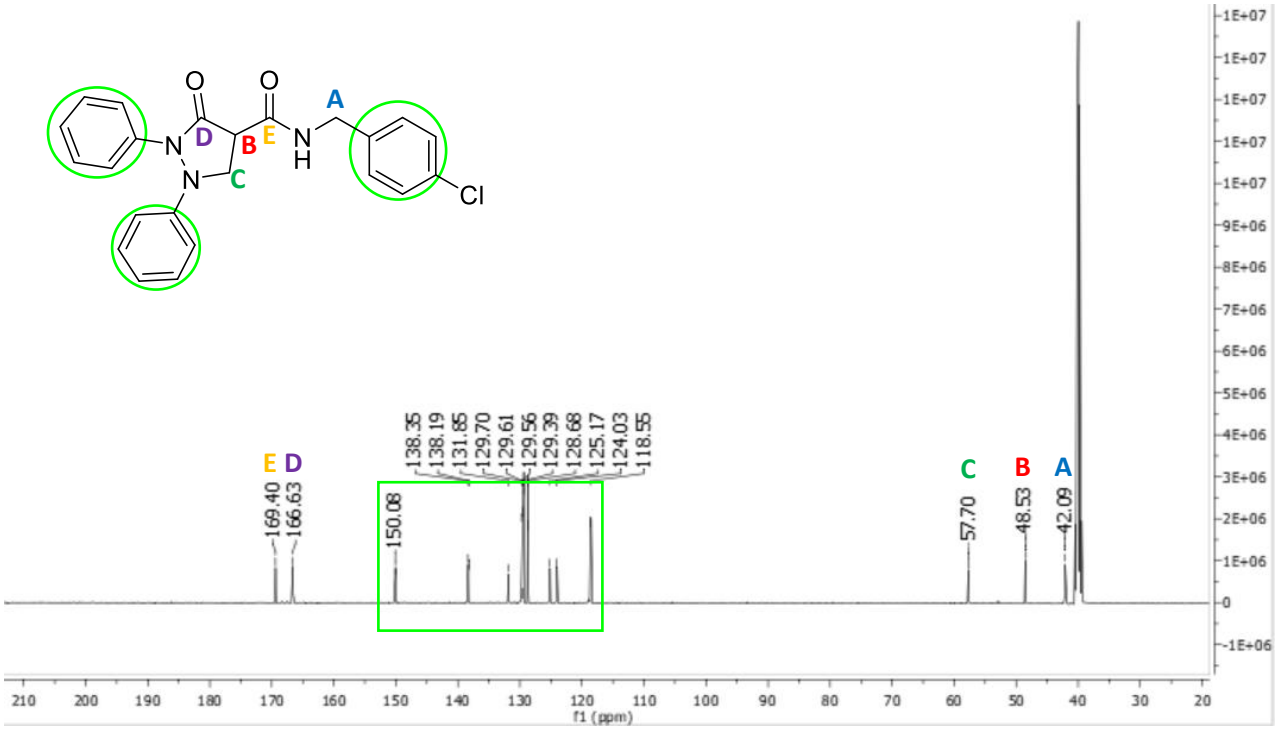
O
O
A
D
E
N
H
B
N
C
Cl
E D
169.40
166.63
138.35
138.19
131.85
129.70
129.61
129.56
129.39
128.68
125.17
124.03
118.55
150.08
C
B
A
57.70
48.53
42.09
f1 (ppm)

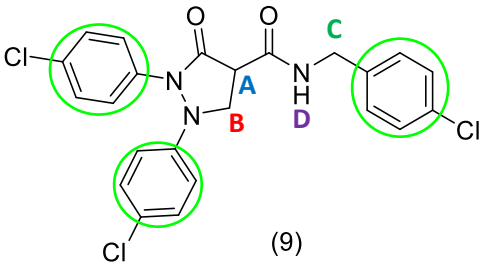
Cl
O
O
C
N
A
N
H
B
D
Cl
Cl

(9)

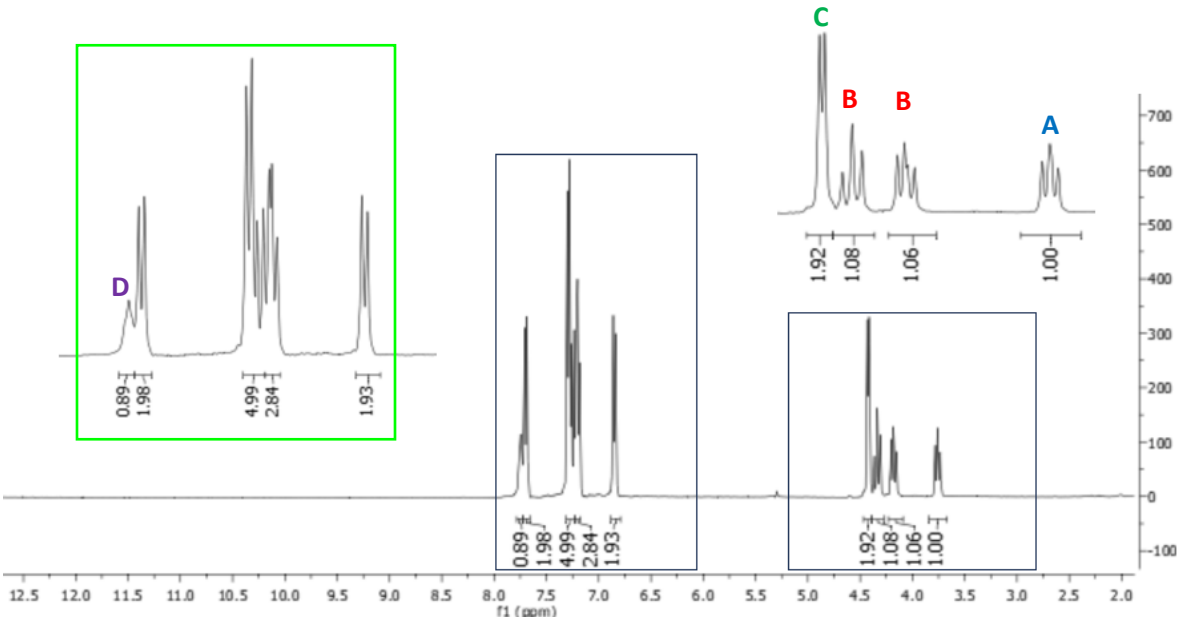
C
B
B
A
D
0.89
1.98
4.99
2.84
1.93
1.92
1.08
1.06
1.00
f1 (ppm)

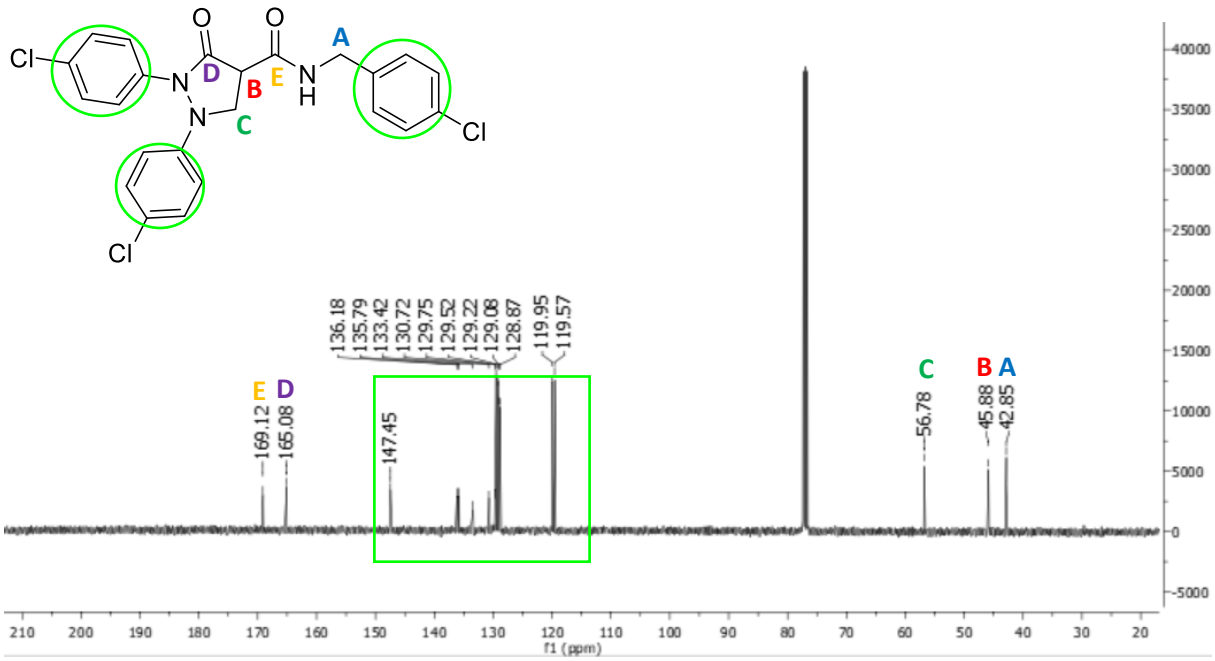
Cl
O
O
A
N
D
B
E
N
H
C
Cl
Cl
136.18
135.79
133.42
130.72
129.75
129.52
129.22
129.08
128.87
119.95
119.57
E
D
169.12
165.08
147.45
C
56.78
B
A
45.88
42.85
f1 (ppm)

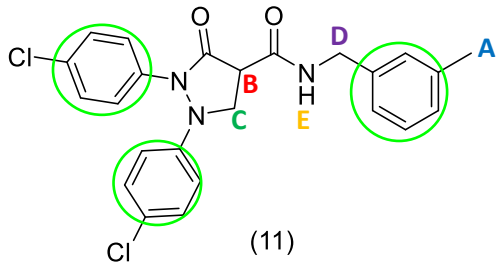
Cl
O
O
N
N
B
C
D
N
H
E
A
Cl

(11)

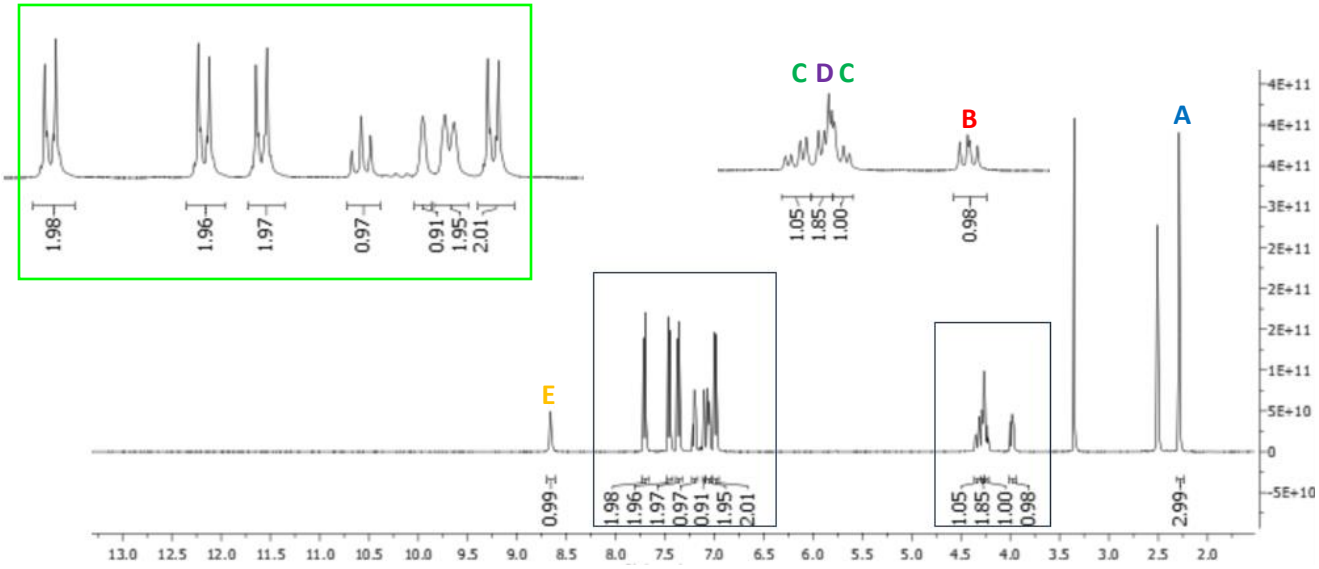
C D C
B
A
E
1.98
1.96
1.97
0.97
0.91
1.95
2.01
1.05
1.85
1.00
0.98
0.99
2.99
13.0 12.5 12.0 11.5 11.0 10.5 10.0 9.5 9.0 8.5 8.0 7.5 7.0 6.5 6.0 5.5 5.0 4.5 4.0 3.5 3.0 2.5 2.0

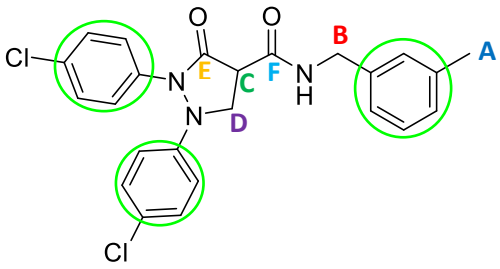
Cl
O
O
N
E
C
F
N
H
B
A
N
D
Cl

F E
169.52
166.28
148.77
139.03
137.83
136.88
129.60
129.56
128.99
128.69
128.26
128.02
127.96
124.67
120.28
120.15
D
C
B
A
57.62
48.65
42.78
21.49
210 200 190 180 170 160 150 140 130 120 110 100 90 80 70 60 50 40 30 20 10
f1 (ppm)

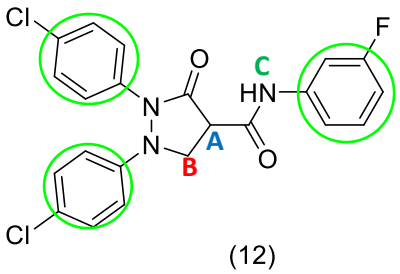
Cl
F
O
C
HN
N
N
A
B
O
Cl

(12)

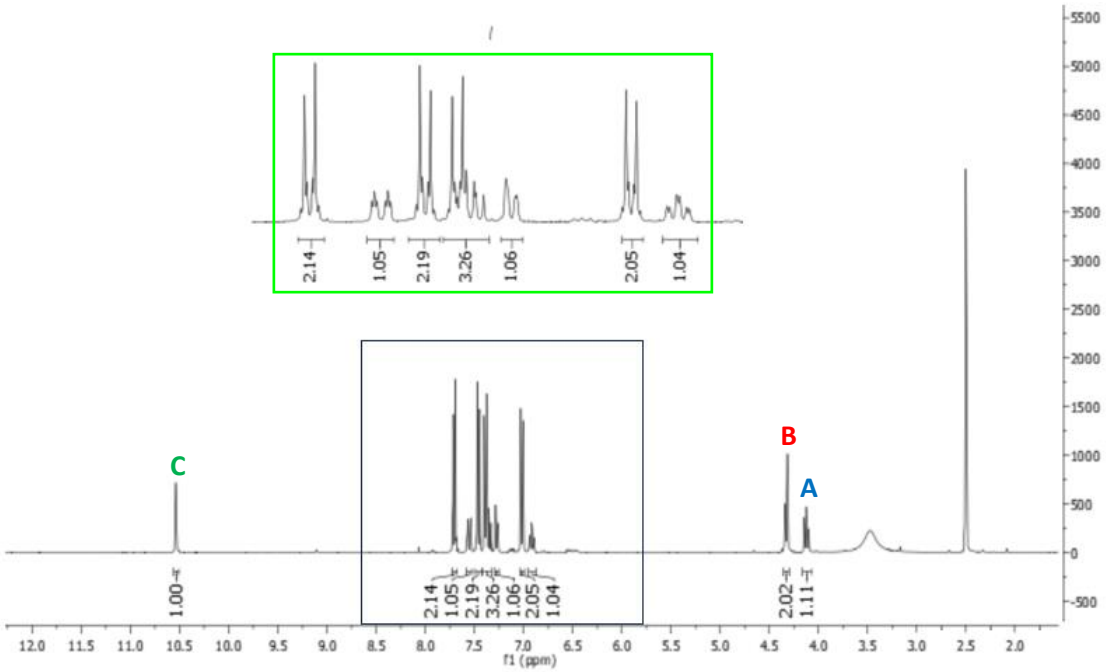
2.14
1.05
2.19
3.26
1.06
2.05
1.04
C
B
A
1.00
2.14
1.05
2.19
3.26
1.06
2.05
1.04
2.02
1.11
f1 (ppm)

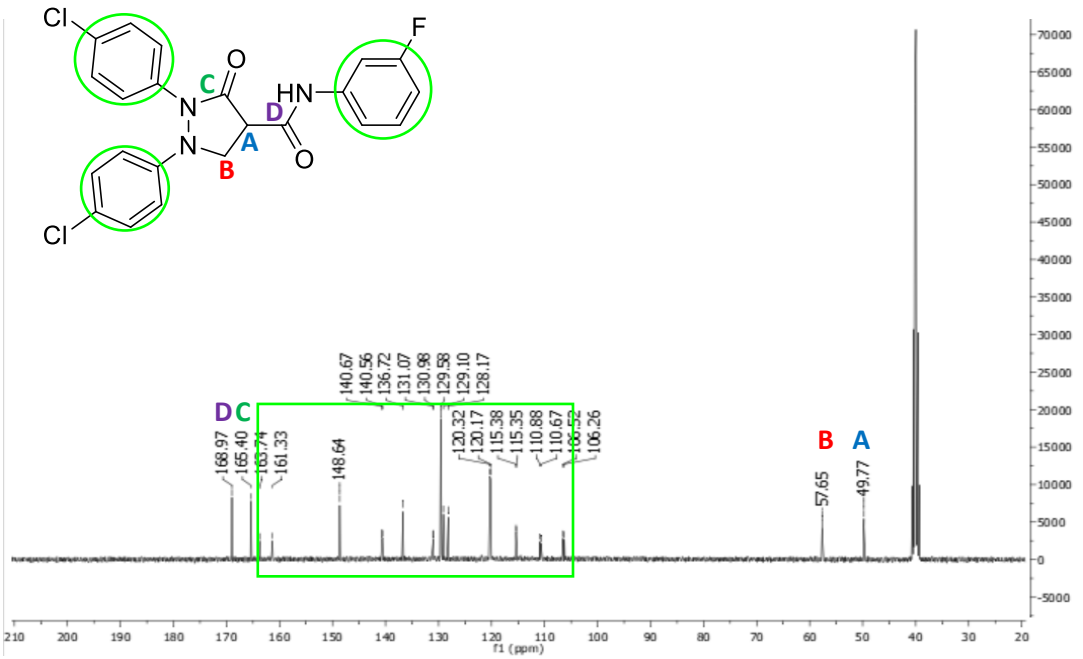
Cl
F
O
C
HN
D
N
N
A
B
O
Cl
D C
B A
f1 (ppm)

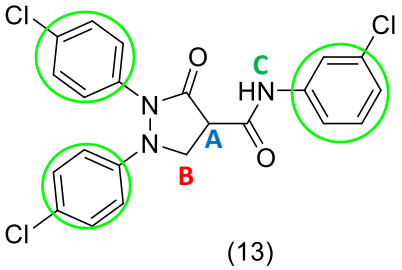
Cl
Cl
O
C
HN
N
N
A
O
B
Cl

(13)

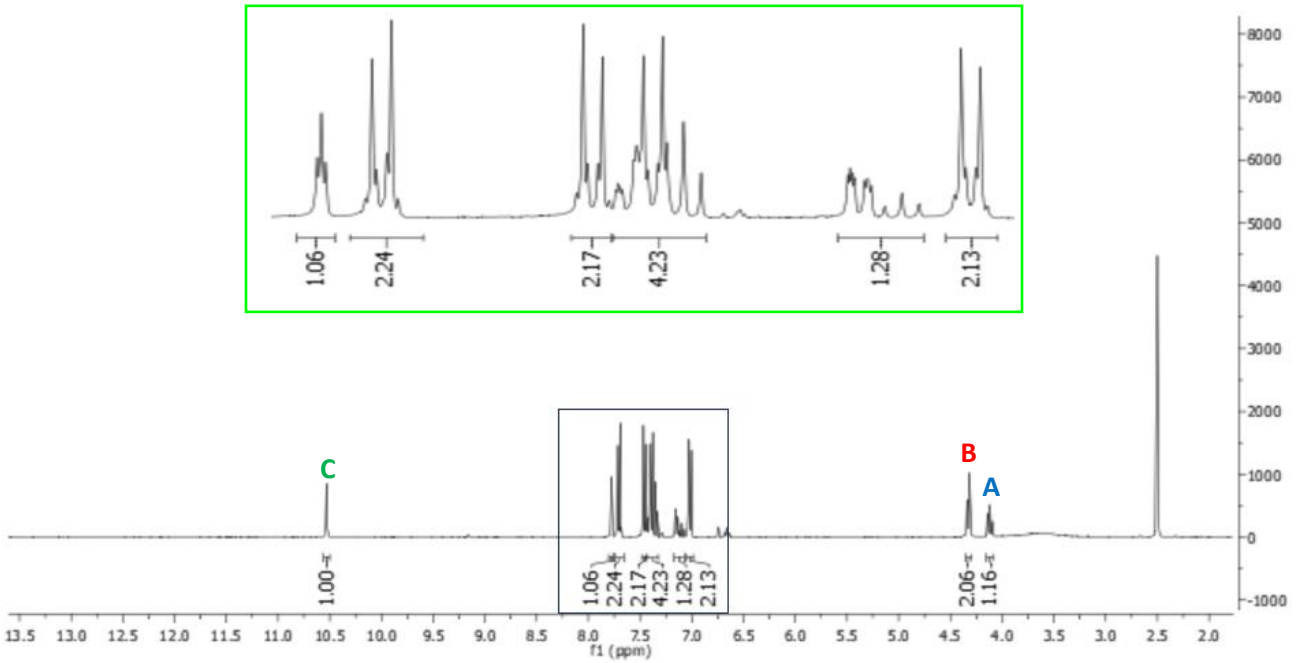
1.06
2.24
2.17
4.23
1.28
2.13
C
B
A
1.00
2.06
1.16
f1 (ppm)

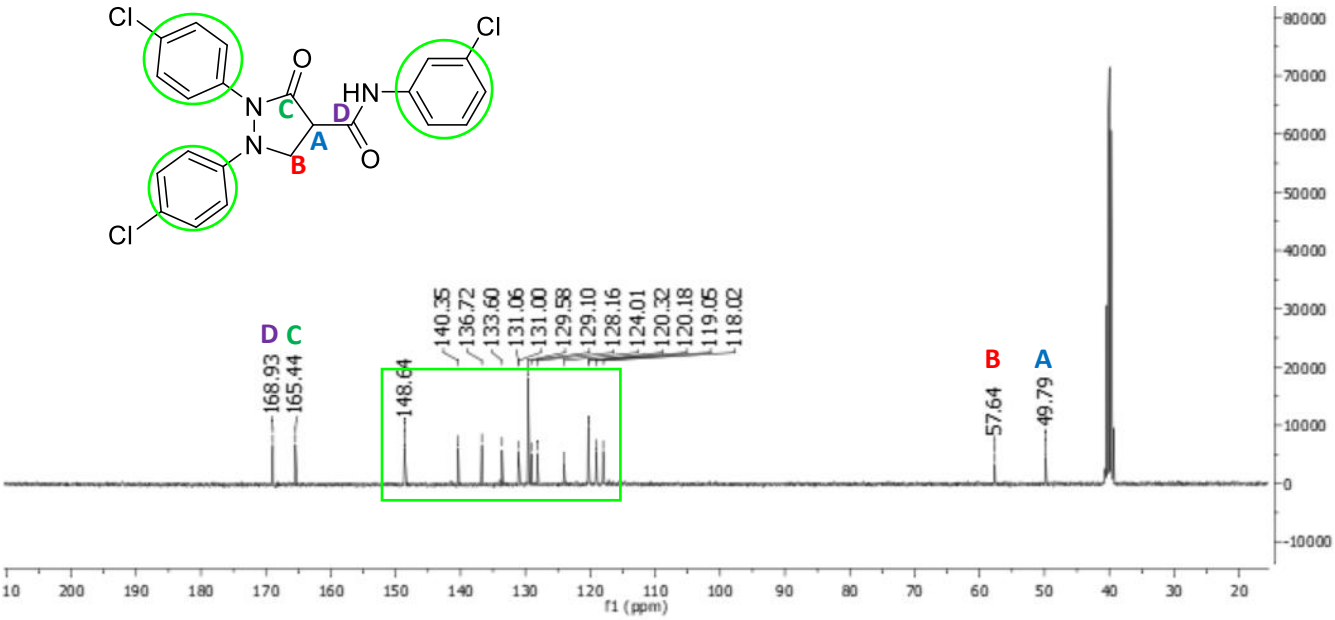
Cl
Cl
O
HN
N
C
D
N
A
B
O
Cl
D C
168.93
165.44
148.64
140.35
136.72
133.60
131.06
131.00
129.58
129.10
128.16
124.01
120.32
120.18
119.05
118.02
B
A
57.64
49.79
f1 (ppm)

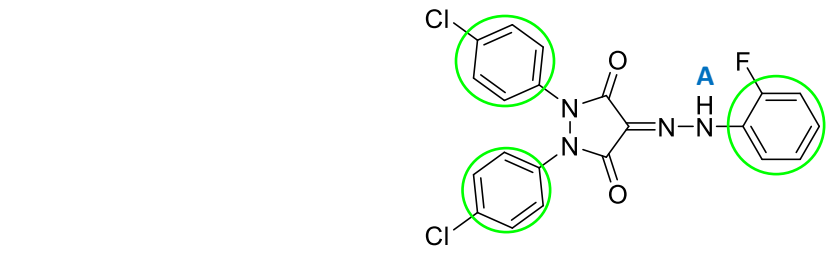
Cl
O
N
N
O
Cl
A
H
N
N
F

(15)

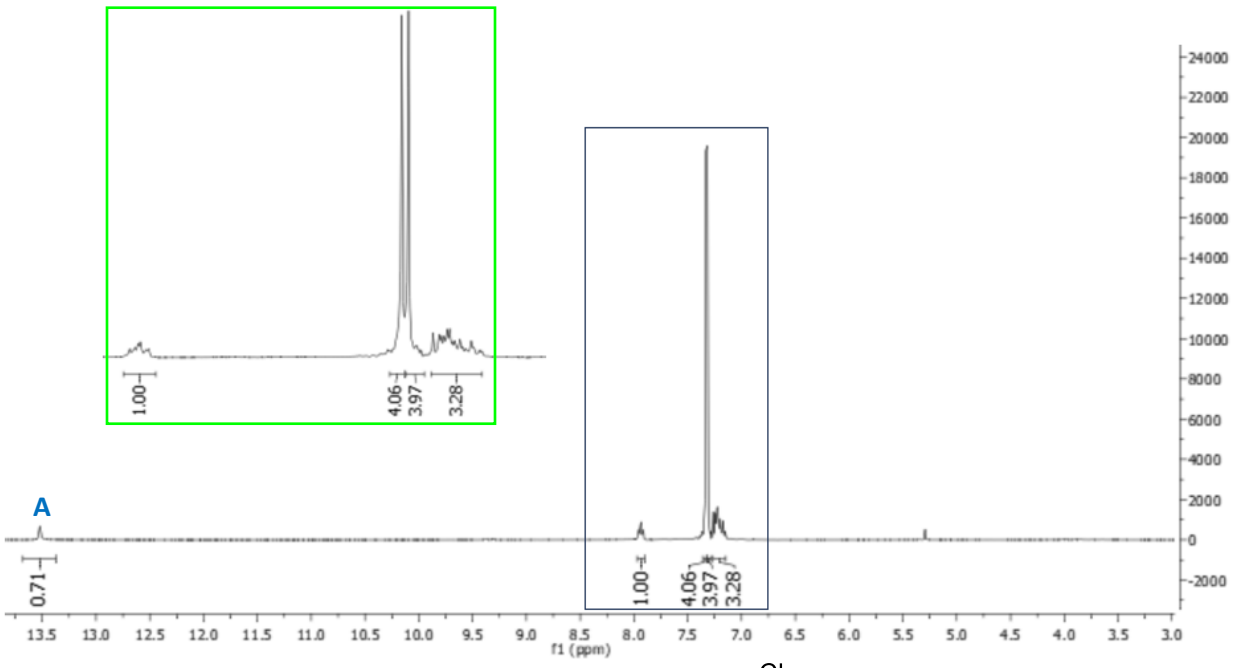
A
1.00
4.06
3.97
3.28
0.71
1.00
4.06
3.97
3.28
f1 (ppm)

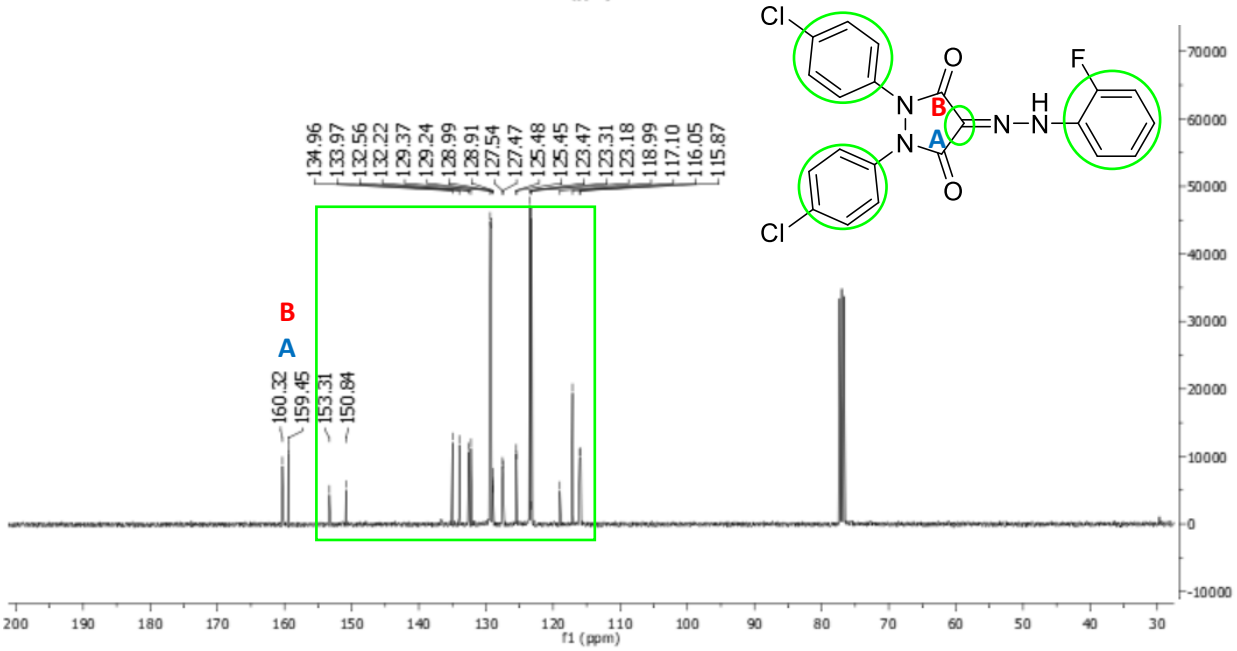
134.96
133.97
132.56
132.22
129.37
129.24
128.99
128.91
127.54
127.47
125.48
125.45
123.47
123.31
123.18
118.99
117.10
116.05
115.87
B
A
160.32
159.45
153.31
150.84
Cl
O
N
B
N
A
O
Cl
H
N
N
F
f1 (ppm)

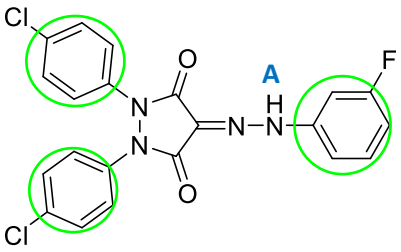
Cl
O
A
F
N
H
N
N
N
O
Cl

(16)

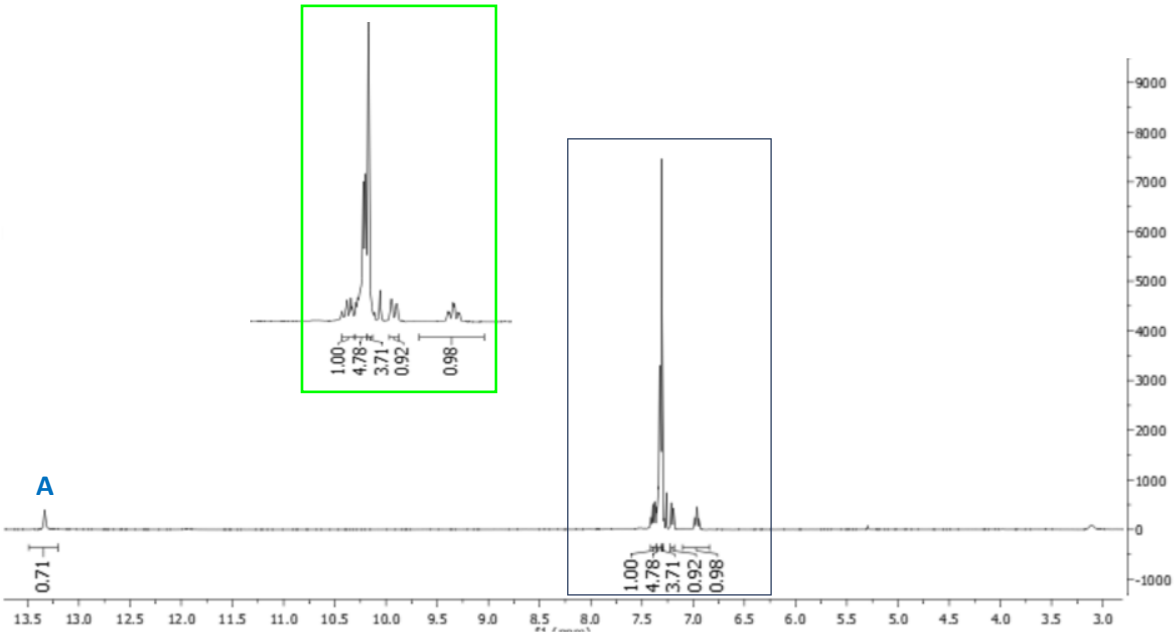
A
1.00
4.78
3.71
0.92
0.98
0.71

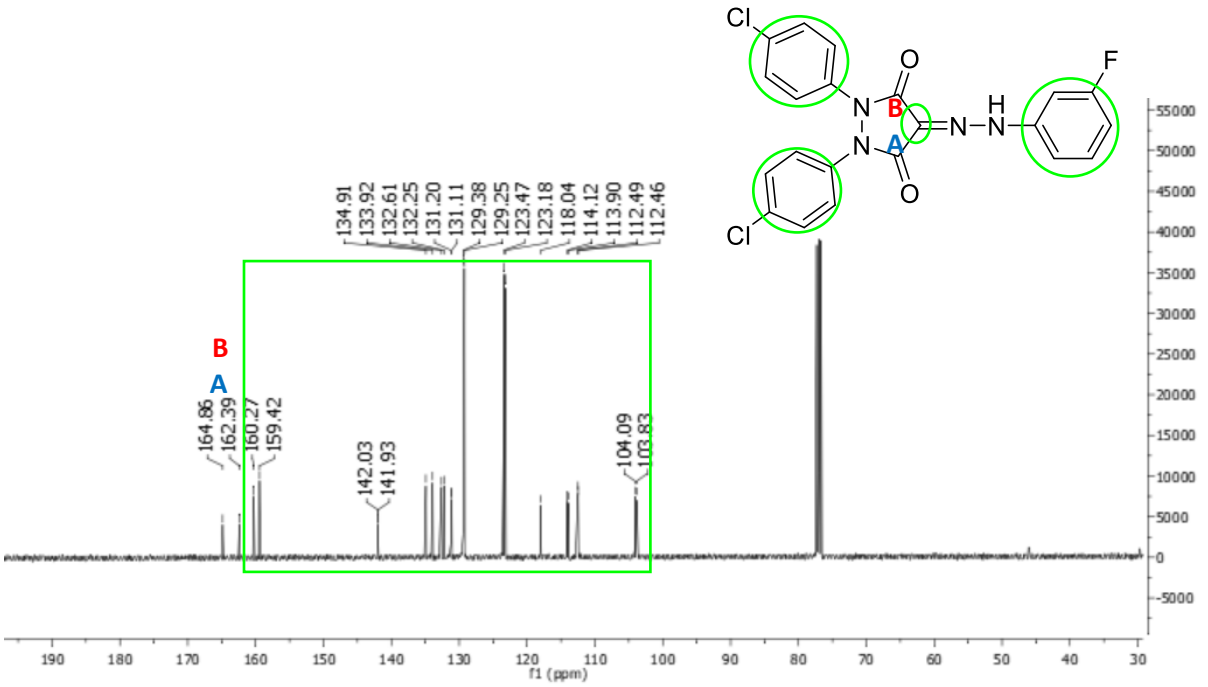
Cl
O
B
F
N
H
N
N
A
O
Cl
134.91
133.92
132.61
132.25
131.20
131.11
129.38
129.25
123.47
123.18
118.04
114.12
113.90
112.49
112.46
B
A
164.86
162.39
160.27
159.42
142.03
141.93
104.09
103.83
f1 (ppm)

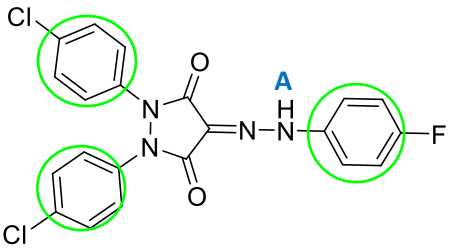
Cl
O
A
H
N
N
N
N
F
Cl
O

(17)

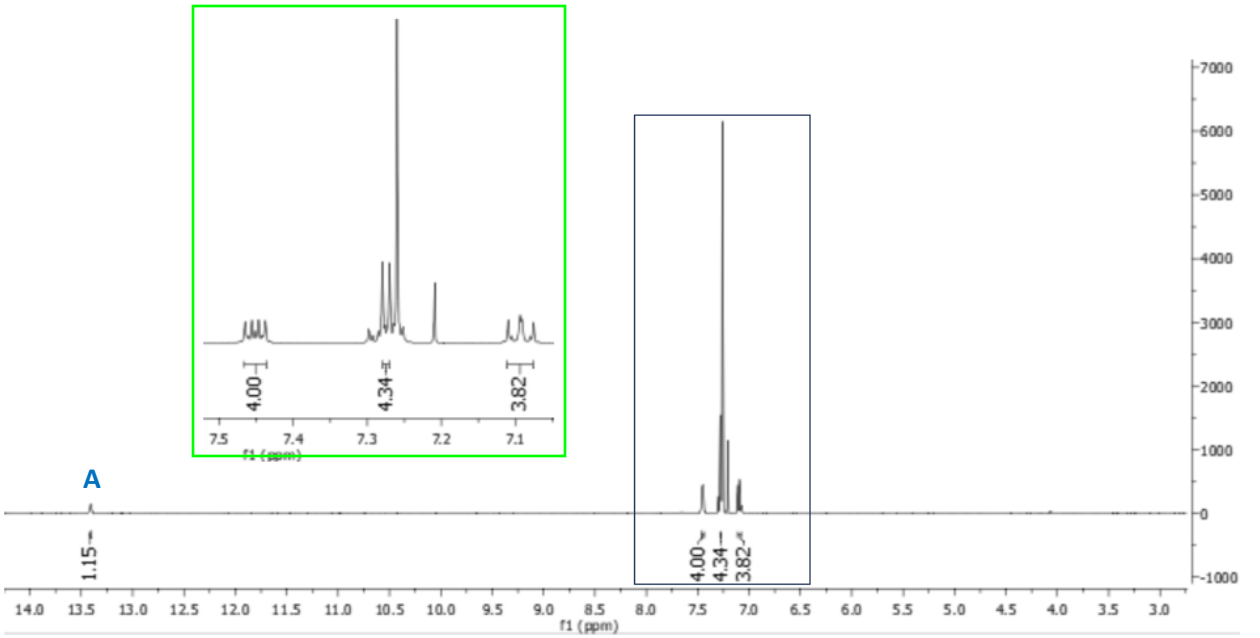
A
4.00
4.34
3.82
1.15
f1 (ppm)

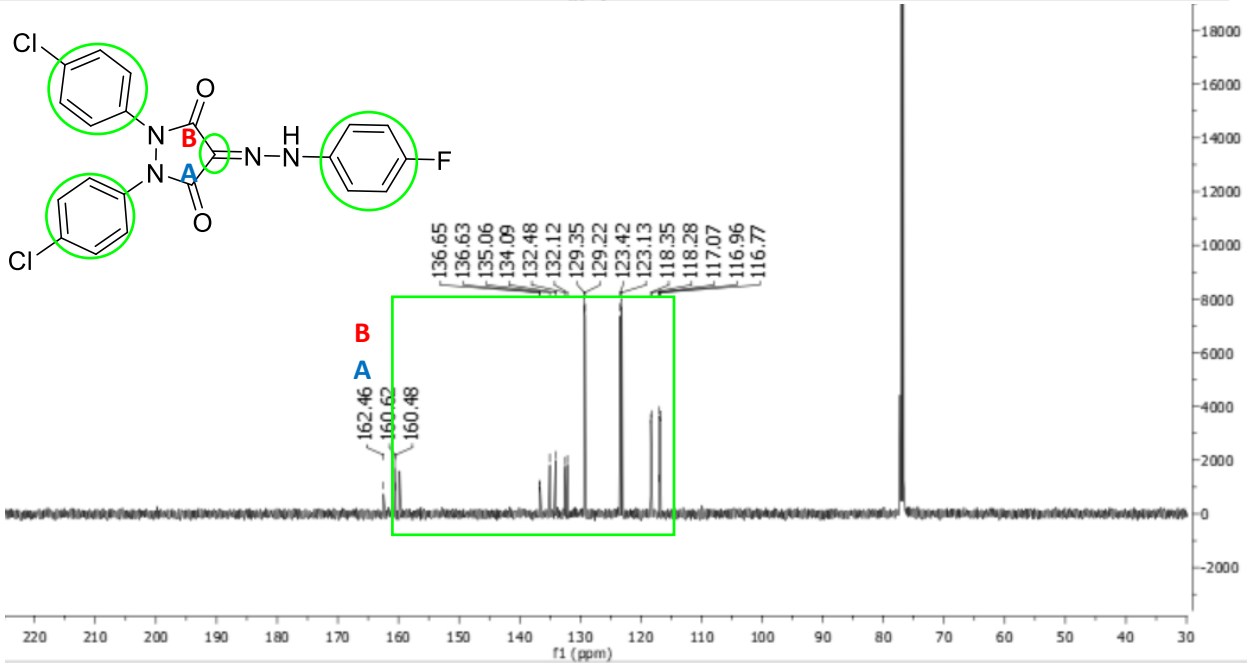
Cl
O
B
N
H
N
N
A
N
F
O
Cl
136.65
136.63
135.06
134.09
132.48
132.12
129.35
129.22
123.42
123.13
118.35
118.28
117.07
116.96
116.77
B
A
162.46
160.62
160.48
f1 (ppm)

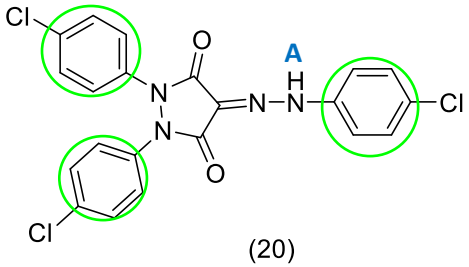
Cl
O
A
H
N
N
N
N
Cl
O
Cl

(20)

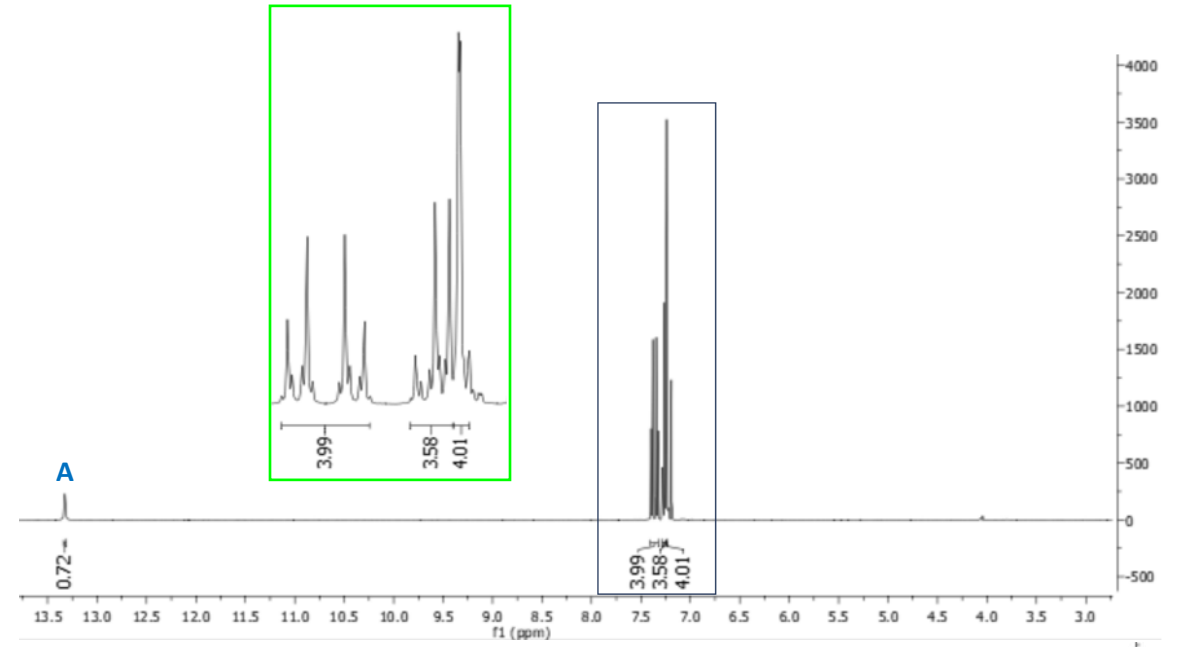
A
3.99
3.58
4.01
0.72
3.99
3.58
4.01
f1 (ppm)

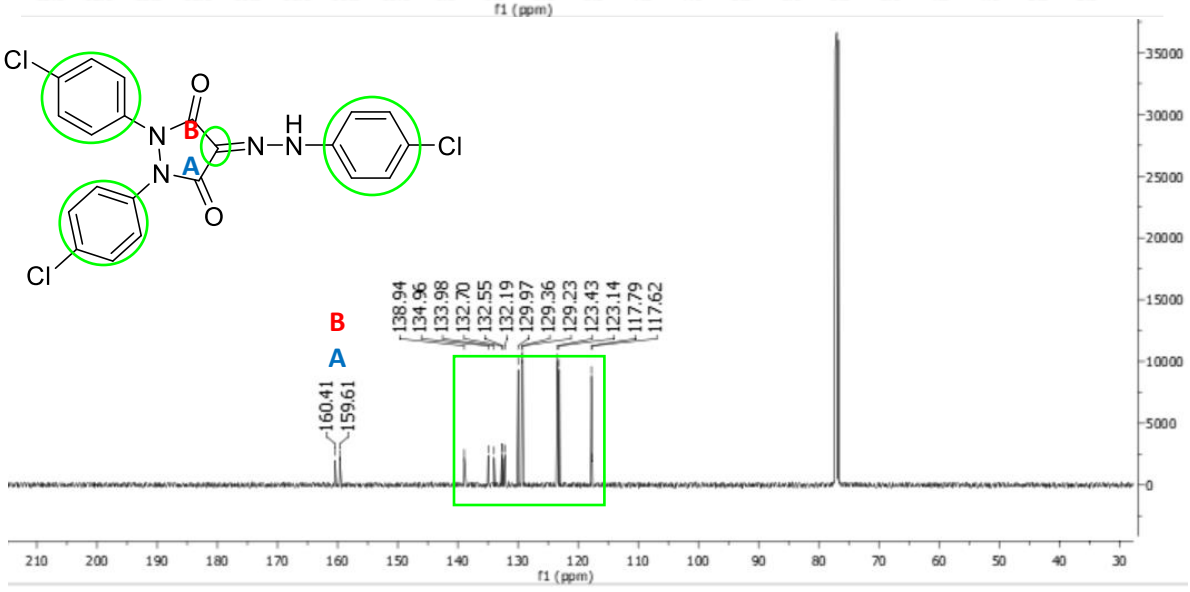
Cl
O
B
A
H
N
N
N
N
Cl
O
Cl
138.94
134.96
133.98
132.70
132.55
132.19
129.97
129.36
129.23
123.43
123.14
117.79
117.62
B
A
160.41
159.61
f1 (ppm)

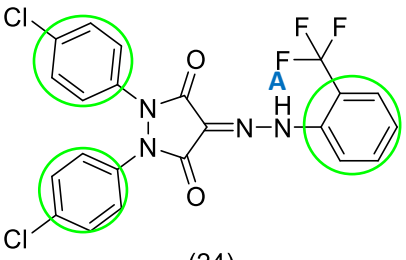
Cl
F F
F
A
H
O
N
N
N
N
O
Cl

(24)

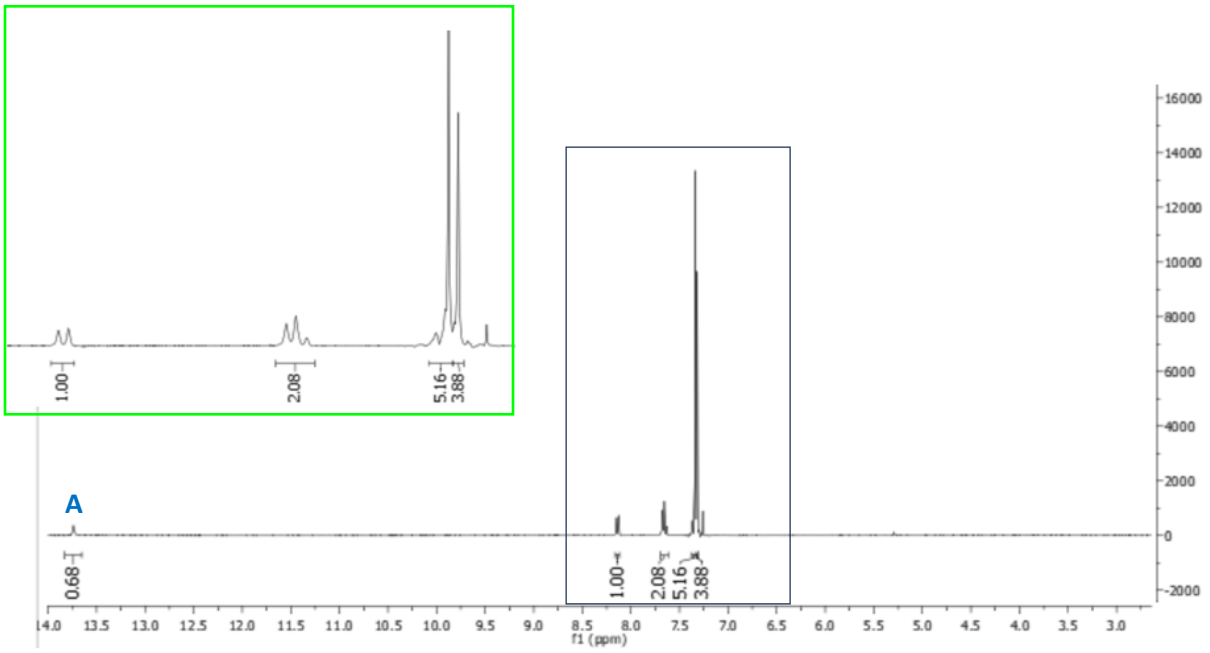
A
1.00
2.08
5.16
3.88
0.68
f1 (ppm)

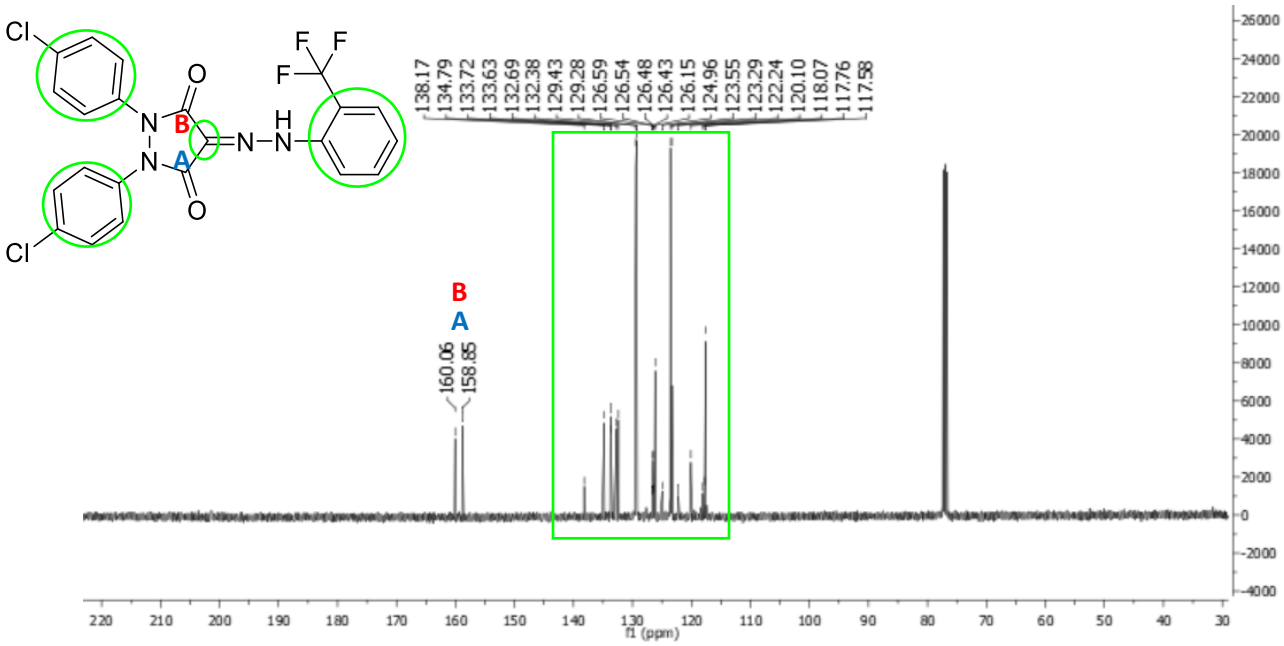
Cl
F F
F
O
N
B
N
A
H
N
N
O
Cl
138.17
134.79
133.72
133.63
132.69
132.38
129.43
129.28
126.59
126.54
126.48
126.43
126.15
124.96
123.55
123.29
122.24
120.10
118.07
117.76
117.58
B
A
160.06
158.85
f1 (ppm)

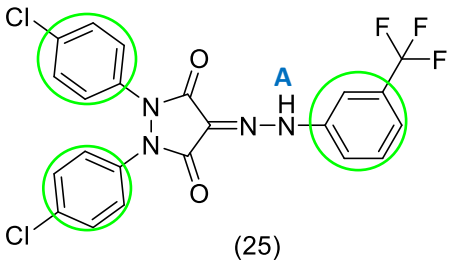
Cl
Cl
O
O
N
N
A
H
N–N
F F
F

(25)

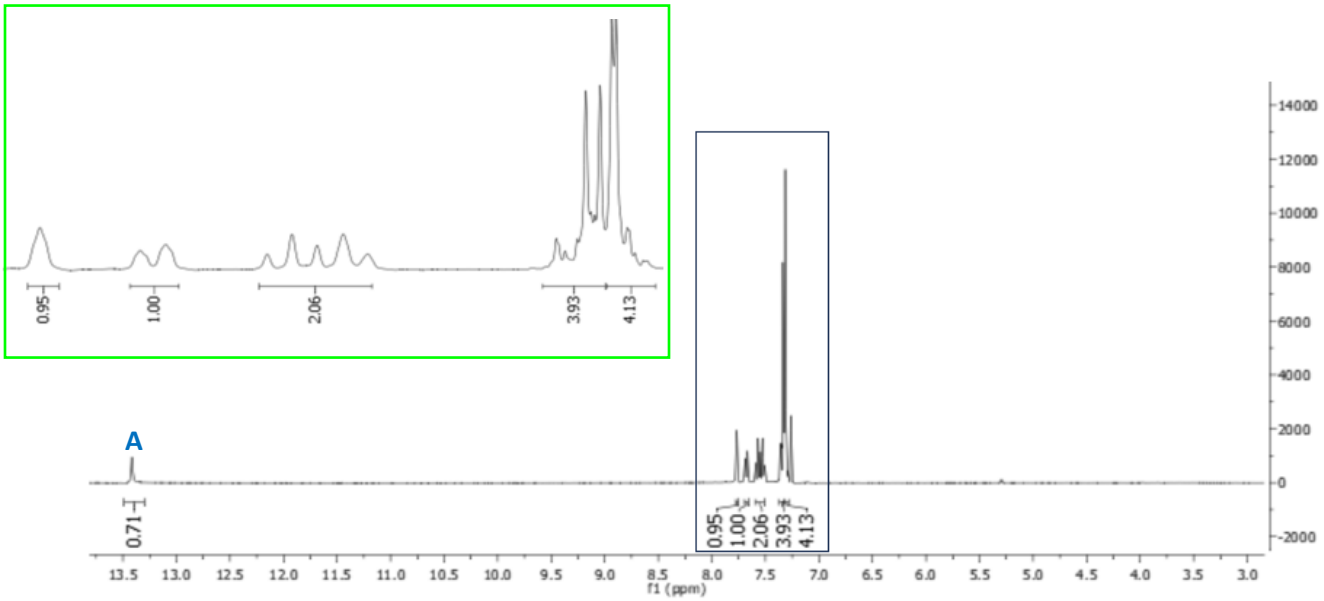
A
0.95
1.00
2.06
3.93
4.13
0.71
f1 (ppm)

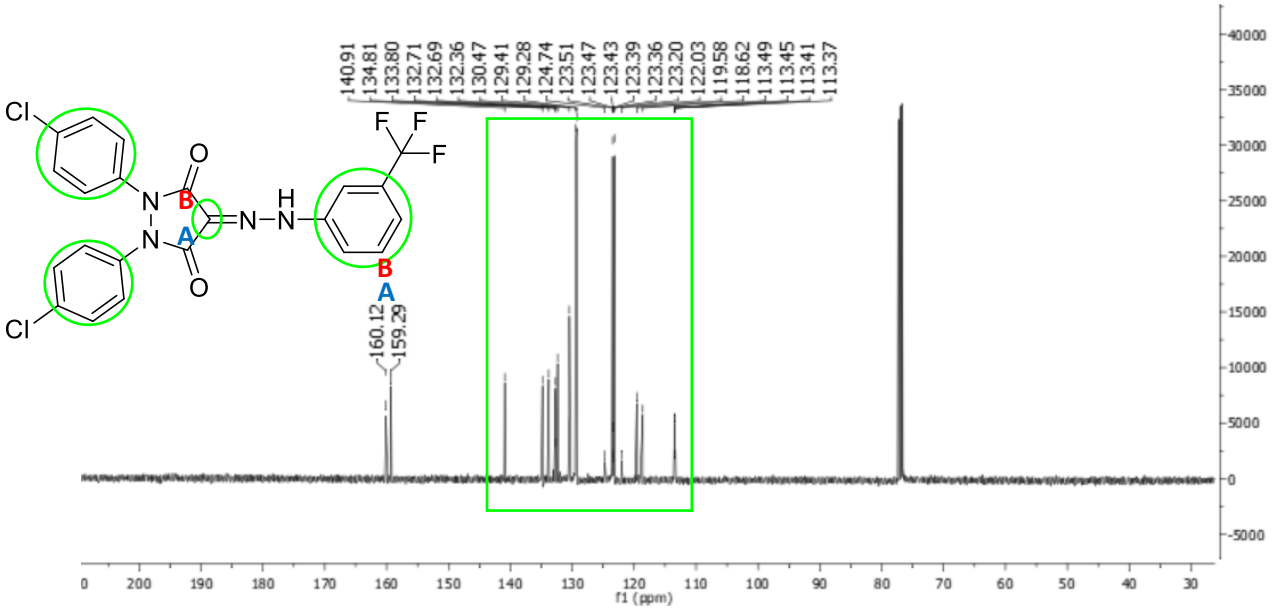
Cl
Cl
O
O
N
N
B
A
H
N–N
F F
F
B
A
160.12
159.29
140.91
134.81
133.80
132.71
132.69
132.36
130.47
129.41
129.28
124.74
123.51
123.47
123.43
123.39
123.36
123.20
122.03
119.58
118.62
113.49
113.45
113.41
113.37
f1 (ppm)

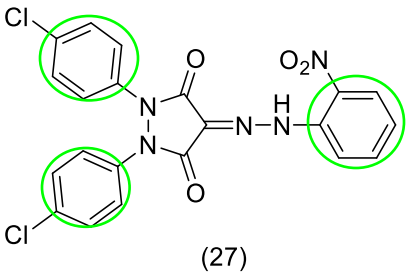
Cl
O
N
N
O
N
H
N
O2N
Cl

(27)

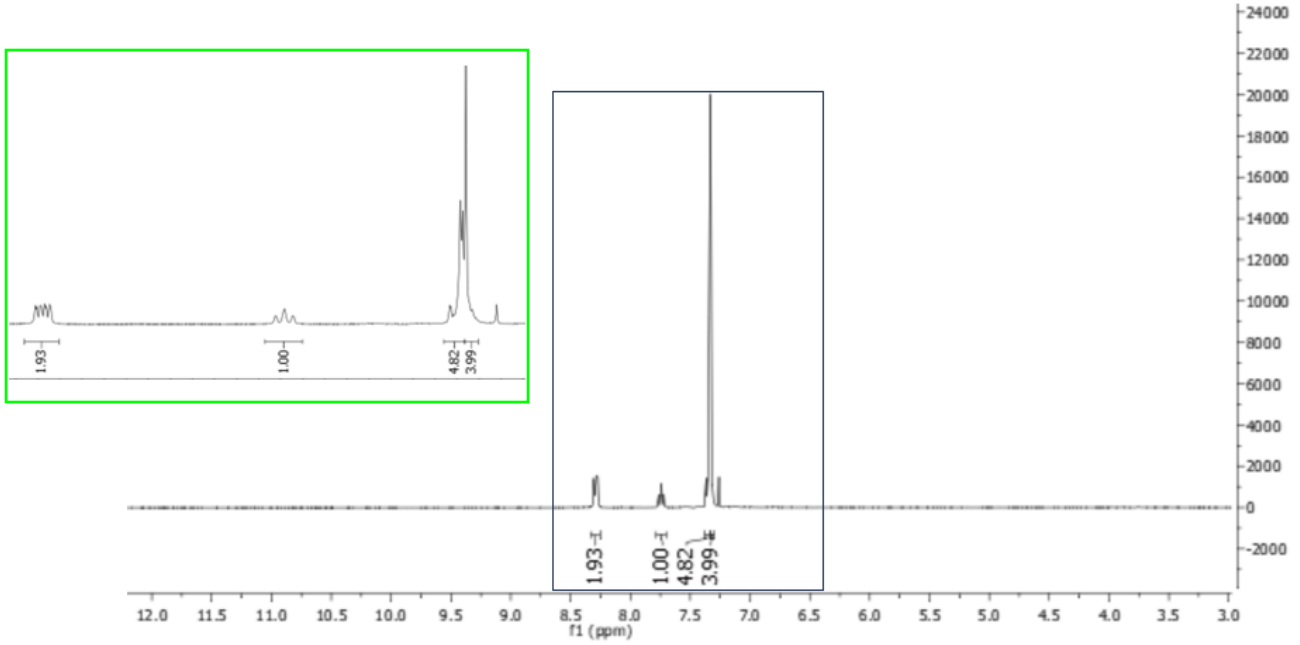
1.93
1.00
4.82
3.99
f1 (ppm)

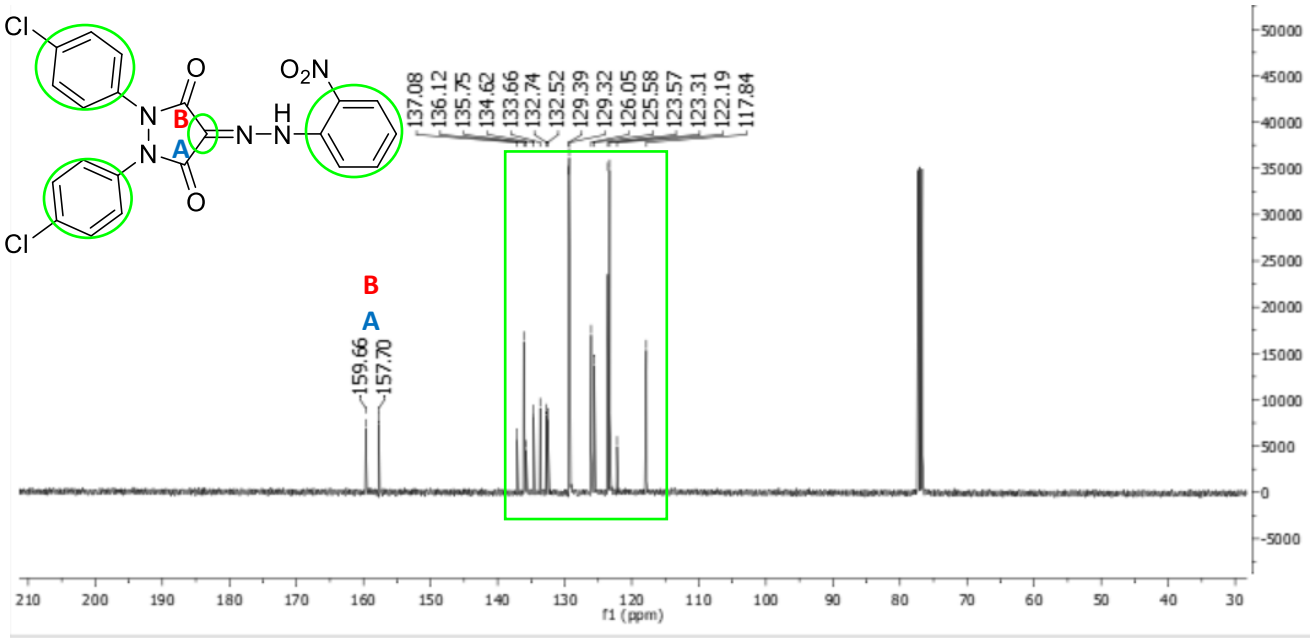
Cl
O
N
B
A
N
N
H
N
O2N
O
Cl
137.08
136.12
135.75
134.62
133.66
132.74
132.52
129.39
129.32
126.05
125.58
123.57
123.31
122.19
117.84
B
A
159.66
157.70
f1 (ppm)

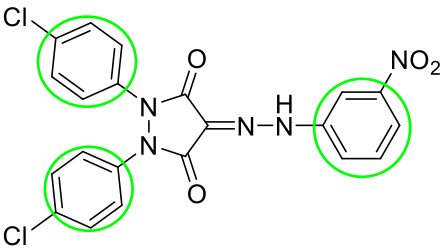
Cl
O
N
N
H
N
N
O
NO2
Cl

(28)

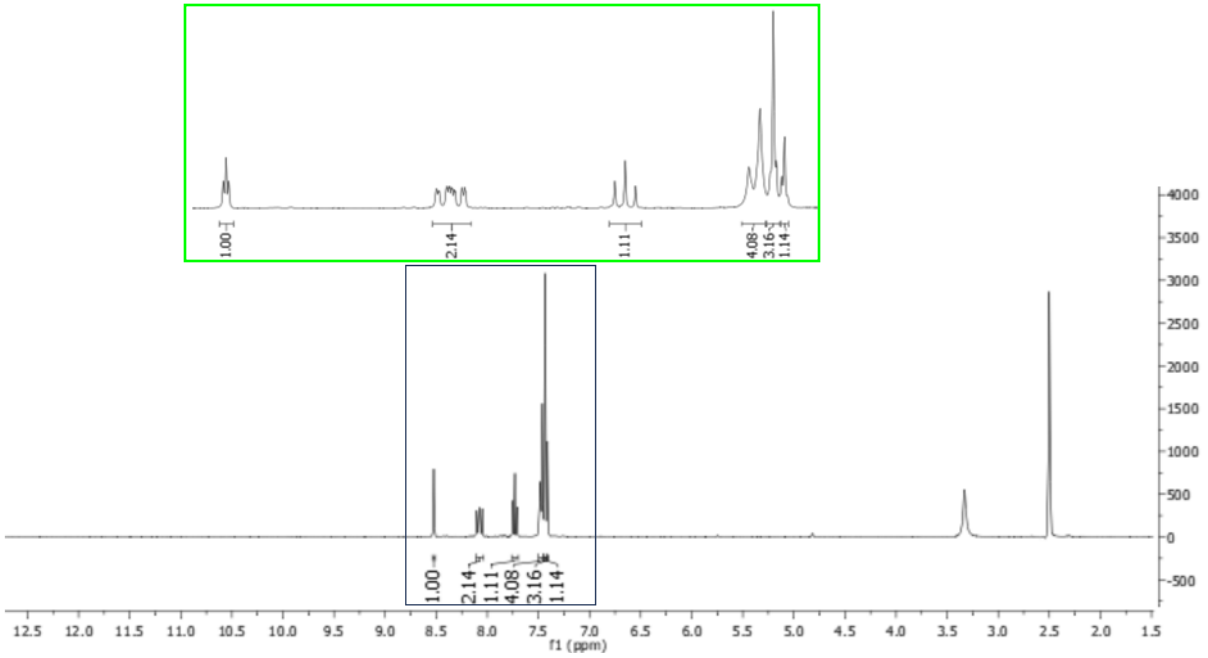
1.00
2.14
1.11
4.08
3.16
1.14
f1 (ppm)

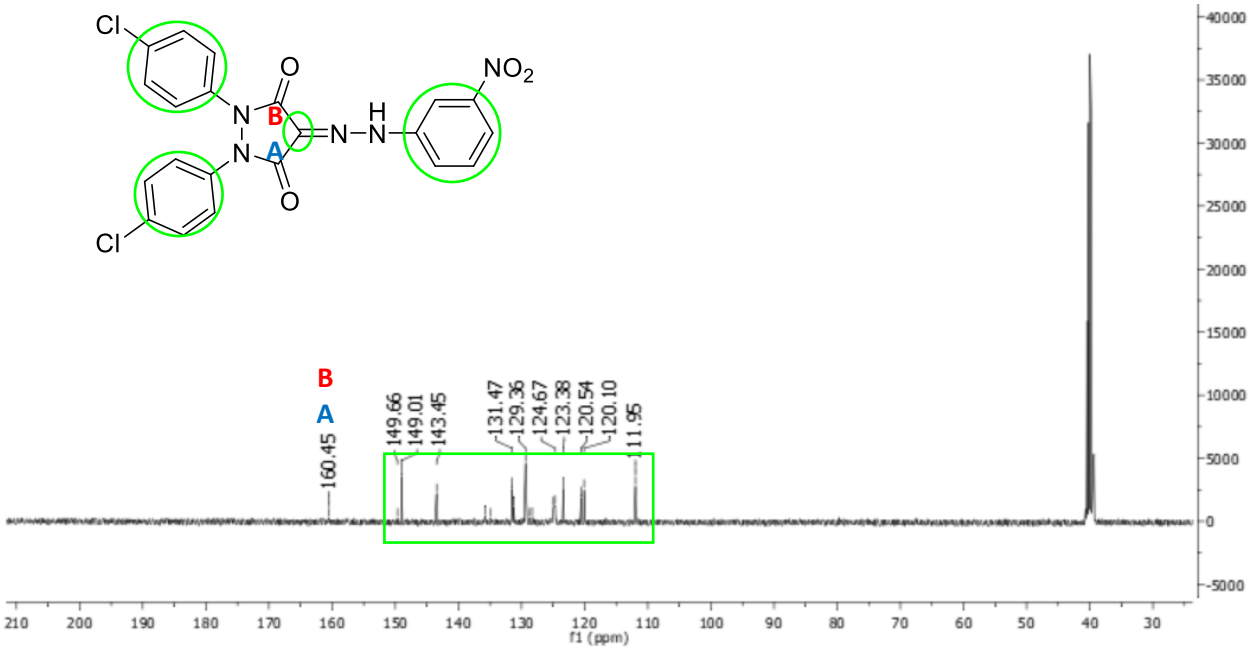
Cl
O
N
B
N
A
H
N
N
O
NO2
Cl
B
A
160.45
149.66
149.01
143.45
131.47
129.36
124.67
123.38
120.54
120.10
111.95
f1 (ppm)

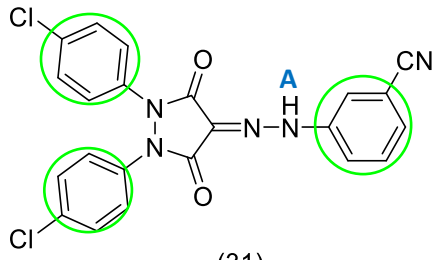
Cl
O
N
N
A
H
N
N
CN
Cl
O

(31)

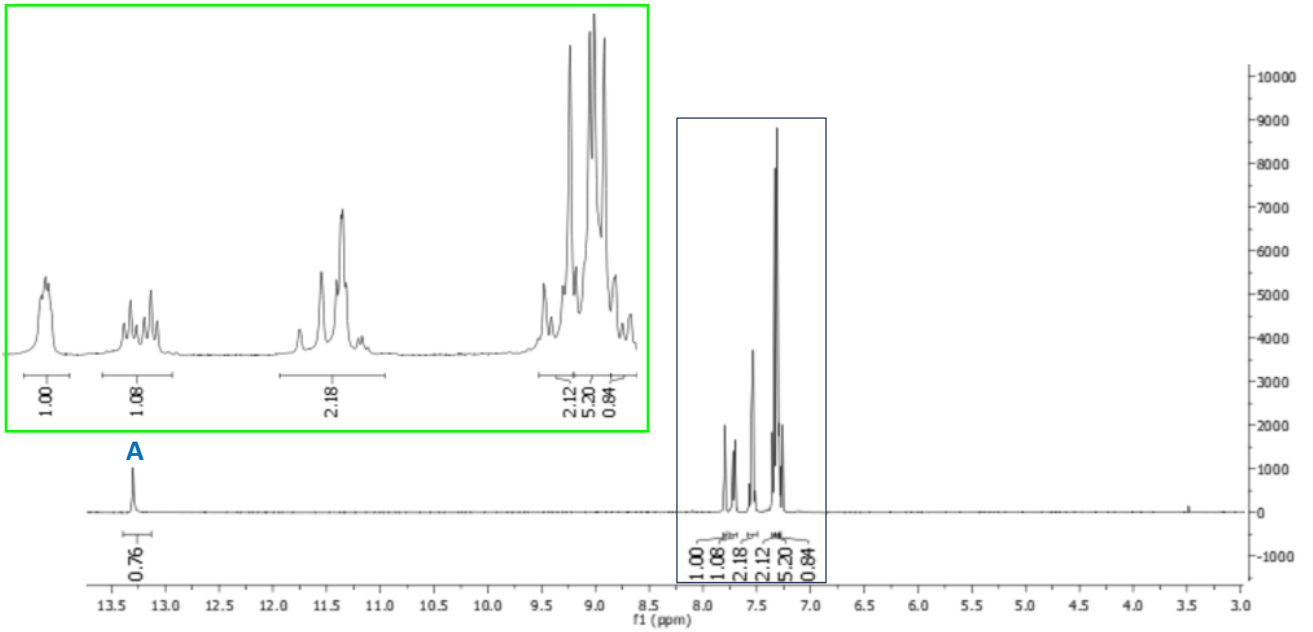
1.00
1.08
2.18
2.12
5.20
0.84
A
0.76
f1 (ppm)

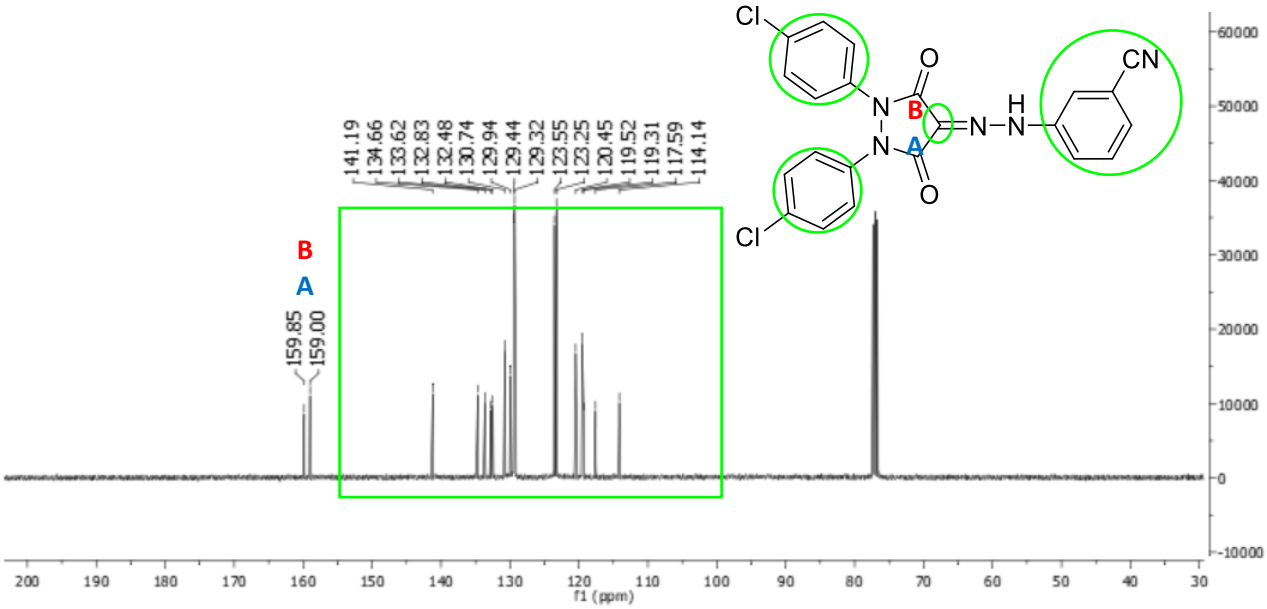
141.19
134.66
133.62
132.83
132.48
130.74
129.94
129.44
129.32
123.55
123.25
120.45
119.52
119.31
117.59
114.14
B
A
159.85
159.00
Cl
O
N
B
N
A
O
H
N
N
CN
Cl
f1 (ppm)

4. Molecular docking simulation:

4.1 Protein preparation

Based on our reported cross docking study [1], For the current molecular docking study in COX-1 and COX-2 enzymes, PDB ID: 5WBE and PDB ID: 3LN1, respectively, were used [2, 3]. The X-ray crystallographic structures of COX-1 and COX-2 enzymes co-crystallized with mofezolac and celecoxib, respectively, as inhibitors (PDB ID: 5WBE and 3LN1, respectively) were downloaded from the protein data bank [4].

Using Discovery Studio Visualizer 2017R2 [5], the target enzymes were prepared for the docking study. Except for chain A, all chains, water molecules and ligands that are not involved in the binding were removed. The GUI "MakeReceptor 3.2.0.2" module from "OEDocking 3.2.0.2" program in OpenEye package was used for additional protein preparation and for defining the active site and the docking box for molecular docking [6-9].

4.2 Ligand preparation

The compounds of interest **15**, **16**, **21**, **24**, and **27-29**, the co-crystalized ligands (mofezolac and celecoxib), were first build as 3D structures using Discovery Studio Visualizer 2017R2 [5]. OMEGA 3.0.0.1 program of OpenEye package was used using *Pose* mode to generate optimal conformers for the subsequent docking pose prediction [10, 11].

4.3 Molecular docking

HYBRID docking protocol from "OEDocking 3.2.0.2" program in OpenEye package was used to perform the molecular docking of the generated conformers of the tested compounds **15**, **16**, **21**, **24**, and **27-29** as well as the co-crystalized ligands in COX-1 and COX-2 active sites using *Chemgauss4* scoring function [8, 9].

The docking protocol was first validated by self-docking of the co-crystallized ligands mofezolac and celecoxib in the active site of COX-1 and COX-2 enzymes, respectively, generating docking poses with energy score (S) and RMSD of −11.13 kcal/mol and 1.915Å, respectively, and −15.37 kcal/mol and 0.913Å, respectively. Moreover, the generated mofezolac and celecoxib docking poses were able to reproduce the key interactions between their experimental poses and COX-1 and COX-2 enzymes, respectively (Table S1 and Figure S3).

Table S1. Docking Score (*S*) and RMSD of the docking poses

Protein	Ligand	Docking score S (kcal/mol)	RMSD (Å)
COX-1 (PDB ID: 5WBE)	Mofezolac	−11.13	1.915
COX-2 (PDB ID: 3LN1)	Celecoxib	−15.37	0.913

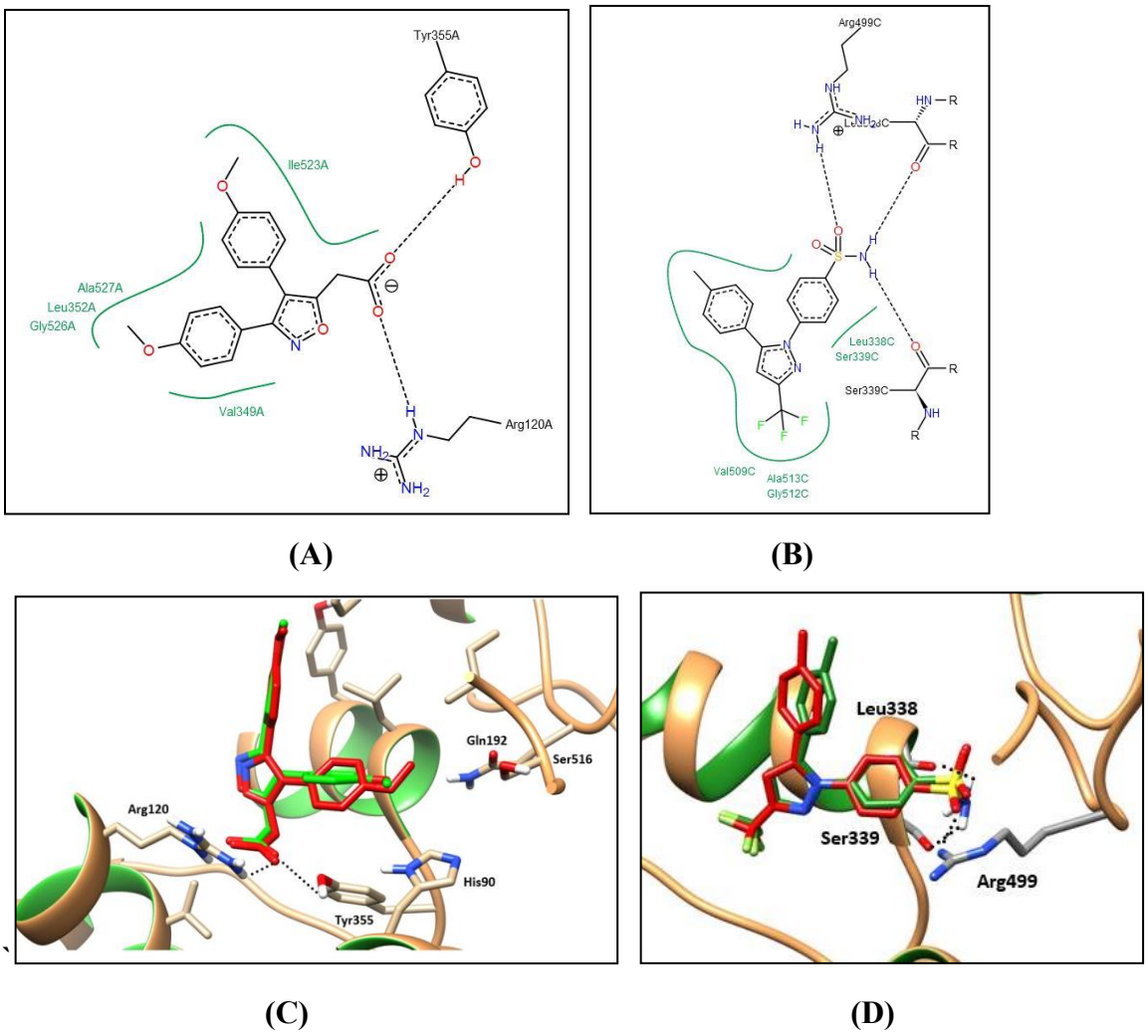

Figure S3. (A) 2D diagrams of the docking pose of mofezolac in COX-1 active site (PDB ID: 5WBE); **(B)** 2D diagrams of the docking pose of celecoxib in COX-2 active site (PDB ID: 3LN1); **(C)** 3D representation of the superimposition of the docking pose (green) and the co-crystallized (red) of mofezolac in COX-1 active site with an RMSD of 1.915Å; **(D)** 3D representation of the superimposition of the docking pose (green) and the co-crystallized (red) of celecoxib in COX-2 active site with an RMSD of 0.913Å. The 2D figures for the ligand-target interactions were generated using PoseView 1.1.2 program [12-15]. The 3D figures were generated using Chimera 1.17.1 [16]

The validated docking setup was then used to dock the target compounds **15**, **16**, **21**, **24**, and **27-29** in the active site of the target enzymes (COX-1 and COX-2).

4.4 Docking poses of the target compounds in COX-1 active site (PDB ID: 5WBE)

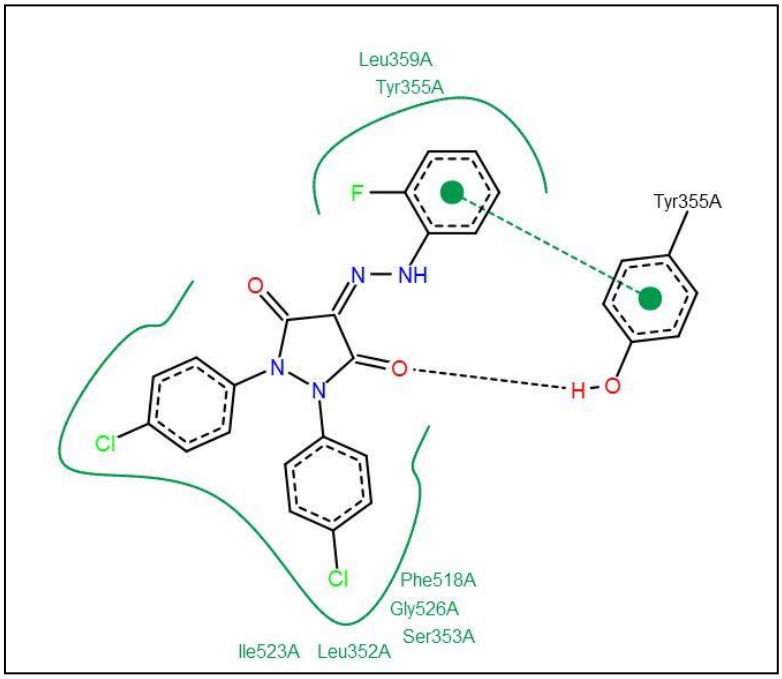

Figure S4. 2D diagram of compound **15** showing its interactions in COX-1 enzyme active site.

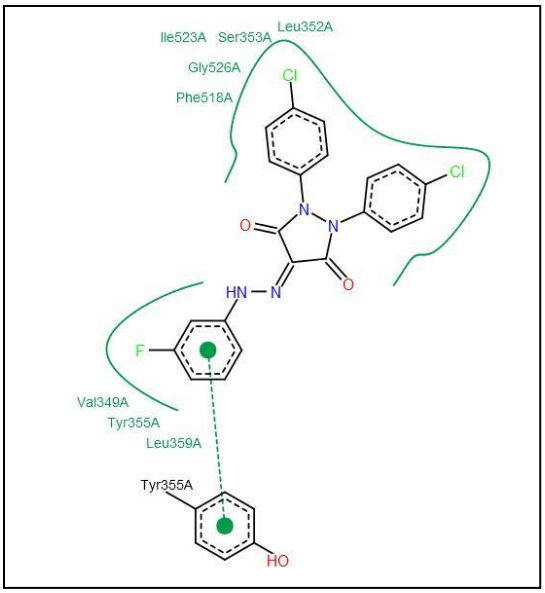

Figure S5. 2D diagram of compound **16** showing its interactions in COX-1 enzyme active site.

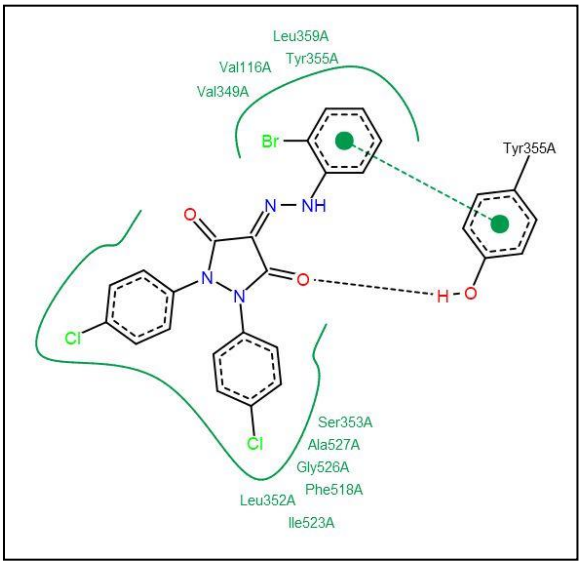

Figure S6. 2D diagram of compound **21** showing its interactions in COX-1 enzyme active site.

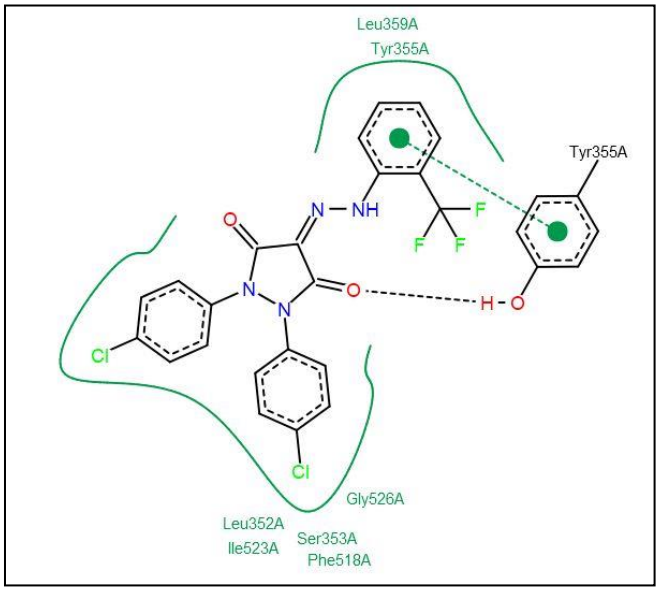

Figure S7. 2D diagram of compound **24** showing its interactions in COX-1 enzyme active site.

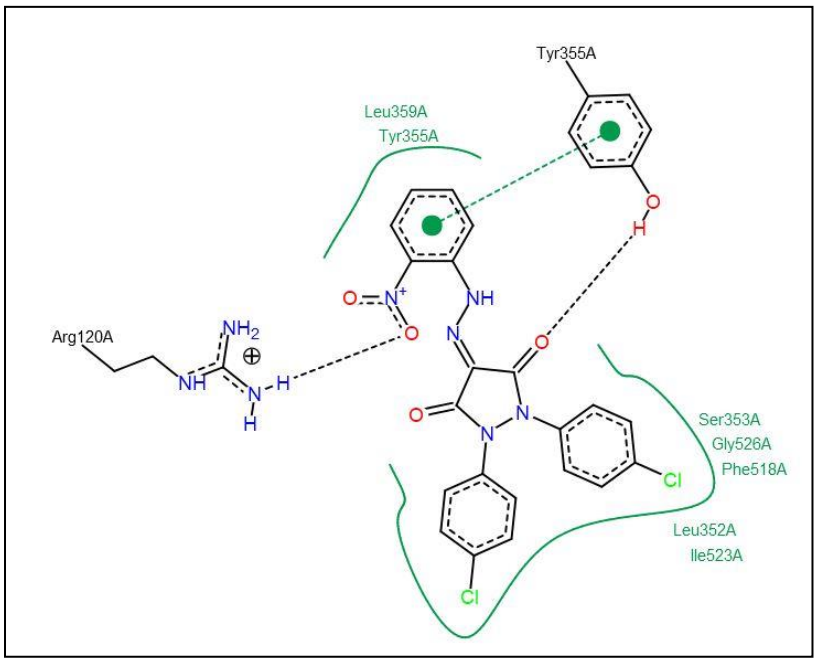

Figure S8. 2D diagram of compound **27** showing its interactions in COX-1 enzyme active site.

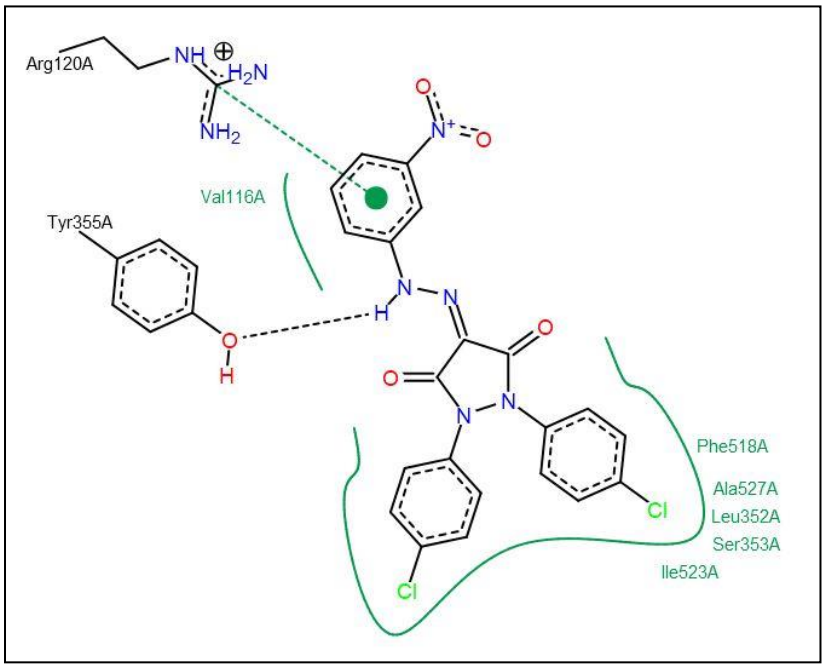

Figure S9. 2D diagram of compound **28** showing its interactions in COX-1 enzyme active site.

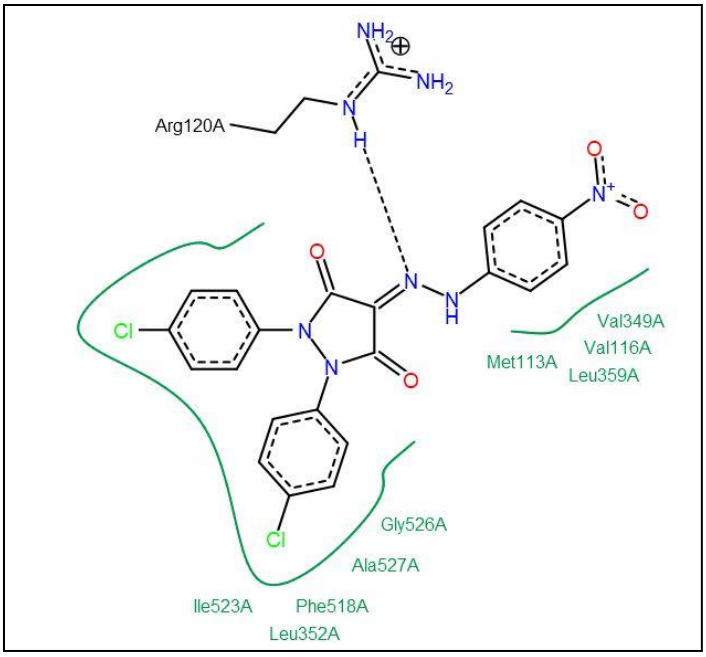

Figure S10. 2D diagram of compound **29** showing its interactions in COX-1 enzyme active site.

4.5 Docking poses of the target compounds in COX-2 active site (PDB ID: 3LN1)

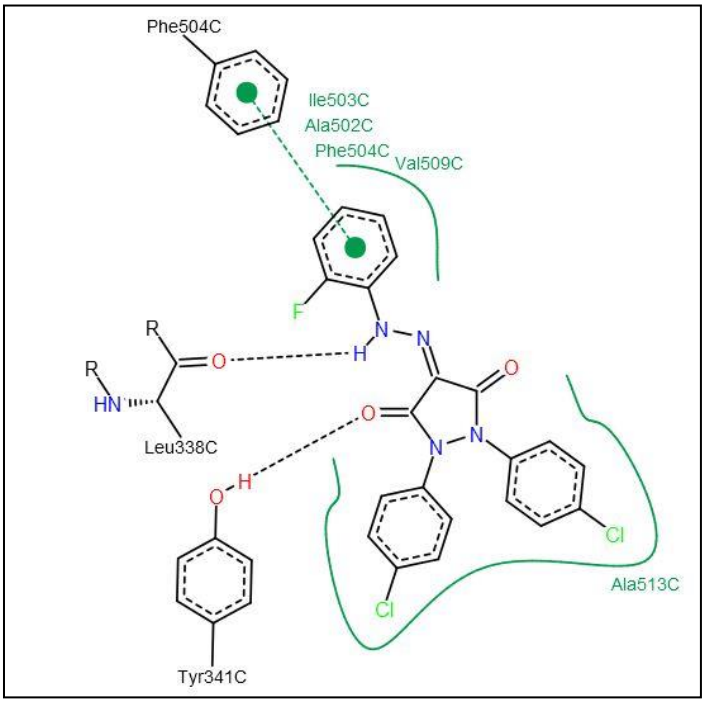

Figure S11. 2D diagram of compound **15** showing its interactions in COX-2 enzyme active site.

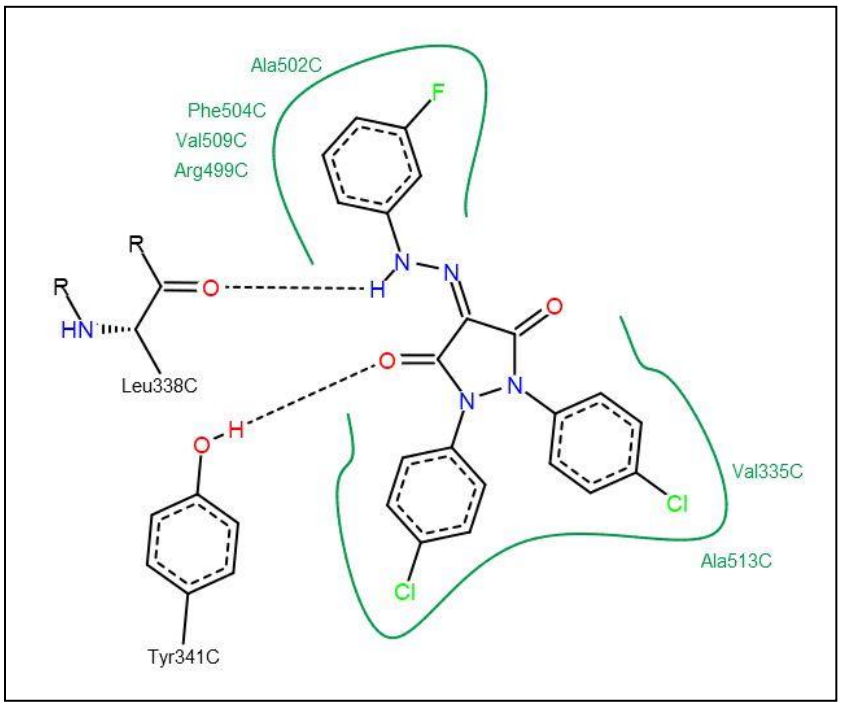

Figure S12. 2D diagram of compound **16** showing its interactions in COX-2 enzyme active site.

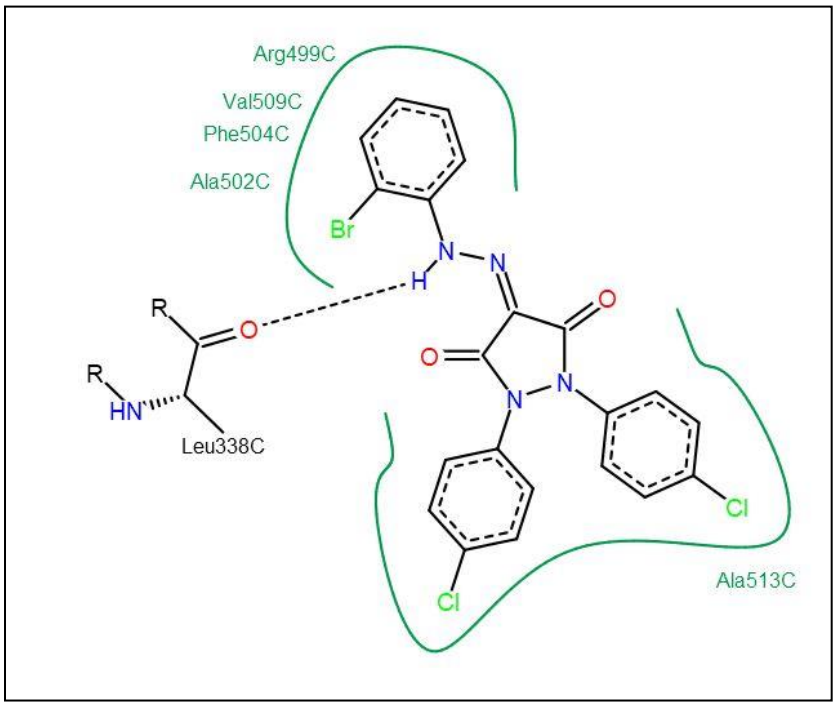

(A)

Figure S13. 2D diagram of compound **21** showing its interactions in COX-2 enzyme active site.

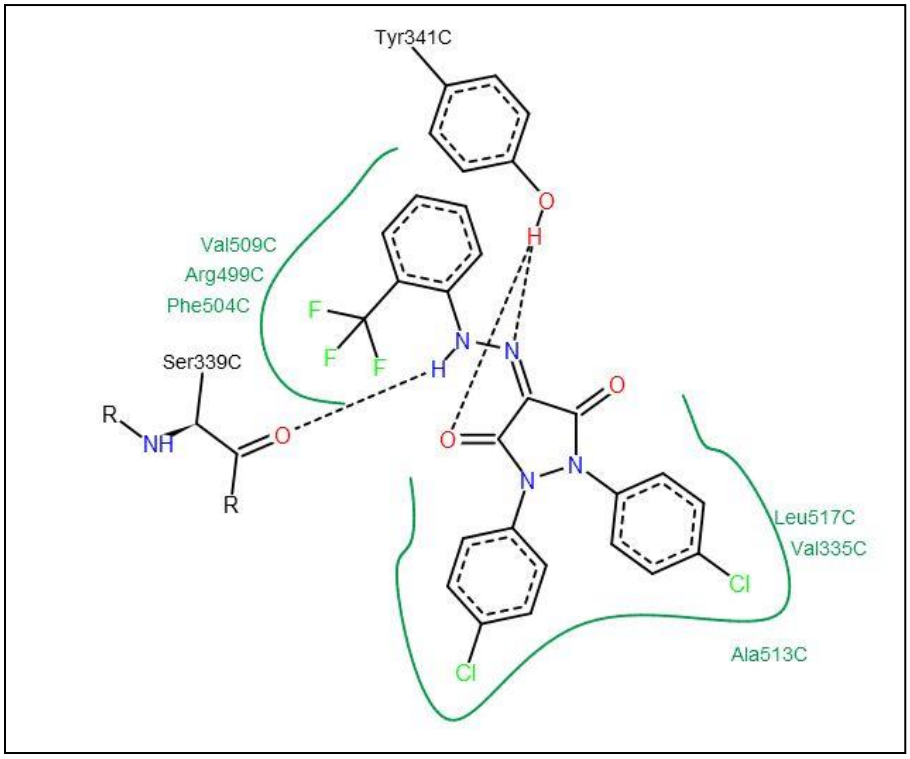

Figure S14. 2D diagram of compound **24** showing its interactions in COX-2 enzyme active site.

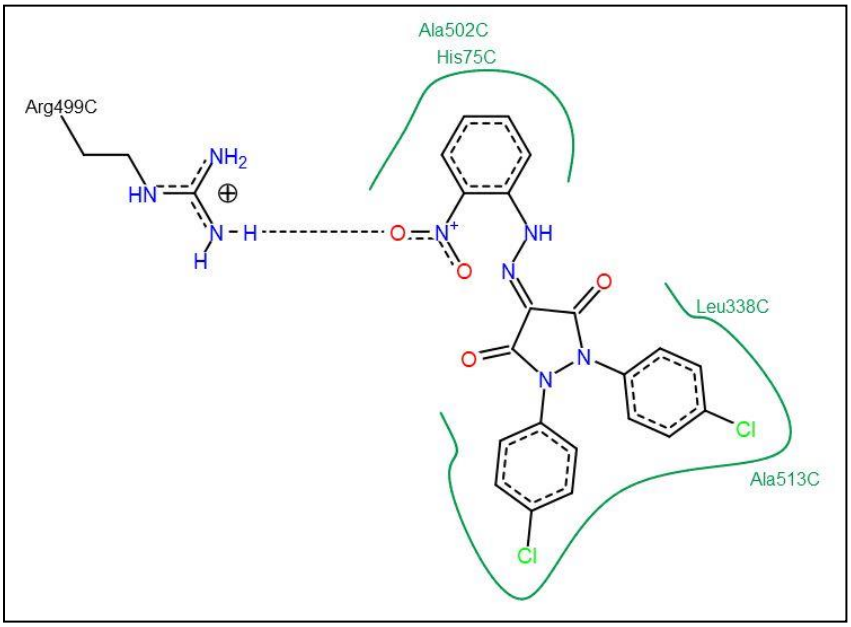

Figure S15. 2D diagram of compound **27** showing its interactions in COX-2 enzyme active site.

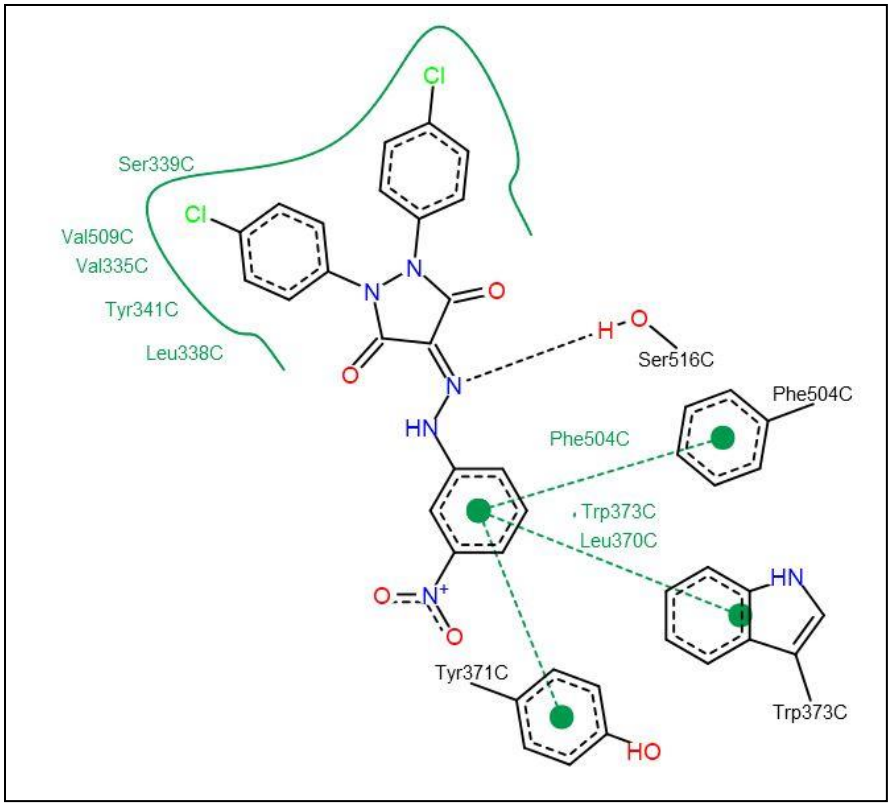

Figure S16. 2D diagram of compound **28** showing its interactions in COX-2 enzyme active site.

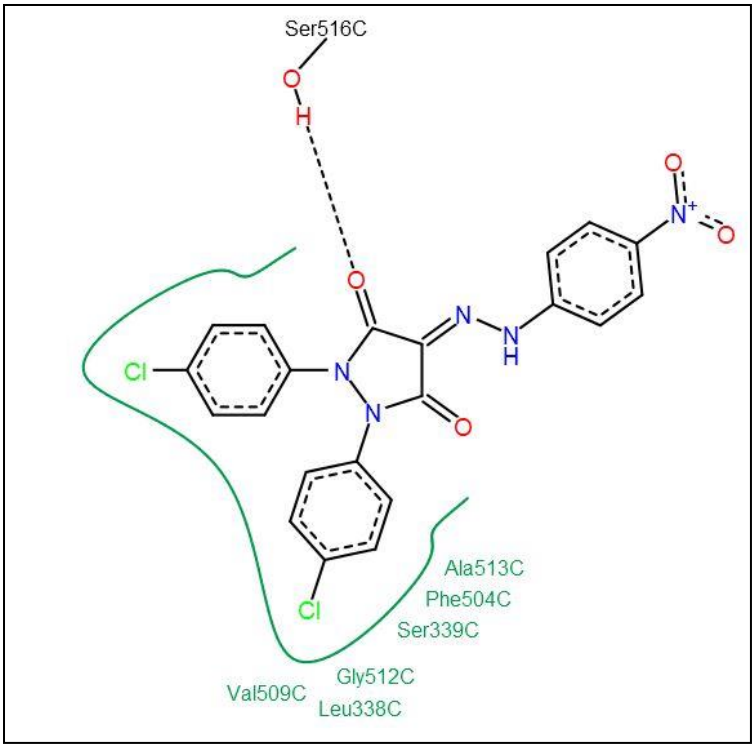

Figure S17. 2D diagram of compound **29** showing its interactions in COX-2 enzyme active site.

5. Molecular dynamic simulations

To further investigate the binding pattern and the dynamic behaviour of the newly synthesized compounds, molecular dynamics (MD) simulations for compound **15**, **16**, and **27**, as representative compounds, in COX-1 and COX-2 active sites were carried out. Starting from the obtained molecular docking complexes of the target compounds in COX-1 and COX-2, MD simulations were performed using Groningen Machine for Chemical Simulations (GROMACS) 2021.3 package [17]. Amber99SB force field was used for protein topology generation [18]. Ligand parametrization was carried out using Amber GAFF force field [19, 20], followed by topology generation using ACPYPE (AnteChamber Python Parser Interface) [21]. Solvation was carried out in a triclinic box (1 nm in all directions from the protein) using TIP3P water model which was neutralized as needed (COX-1 complexes were neutral, whereas two Na^+ ions were used in COX-2 complexes). System energy minimization was first performed using steepest descent algorithm until it converged to F_{max} less than 1000 kJ mol^{-1} nm^{-1}. Then system equilibration was carried out under NVT followed by NPT ensembles, 100 ps each, with the protein

atomic positions restrained. In the NVT step, the modified Berendsen (V-rescale) thermostat with a time constant of 0.1 ps was used to keep the temperature at 300 K [22]. In the NPT step, the pressure was maintained at 1 bar using the Berendsen pressure coupling method (isotropic coupling type) with a time constant of 2 ps [23]. Finally, full production simulations for 100 ns were run using the leap-frog integrator with a timestep of 2 fs. During the production runs, Linear Constraint Solver (LINCS) algorithm, V-rescale thermostat with a time constant of 0.1 ps, and Parrinello−Rahman barostat with a time constant of 2 ps were used [22, 24, 25]. Particle Mesh Ewald summation (PME) method was used for long-range electrostatics description [26]. Long-range electrostatic and short-range van der Waals cut-off was set to 1 nm. Trajectories were recorded after every 10.0 ps. The analysis of the resulting trajectories was performed using GROMACS tools [17] and Chimera 1.17.1 [16]. For both complexes, the Root Mean Square Deviation (RMSD) from the initial reference frame backbone was calculated for the backbone Cα atom and was graphically analysed at a time point scale in ns [27, 28]. Furthermore, root mean square fluctuation (RMSF) for each residue was also calculated [29]. Radius of gyration (Rg) was also calculated to understand the compactness of COX-1 and COX-2 complexes with the target compounds [30].

5.1 RMSD, RMSF, Rg graphs of the MD simulations of the target compounds in COX-1

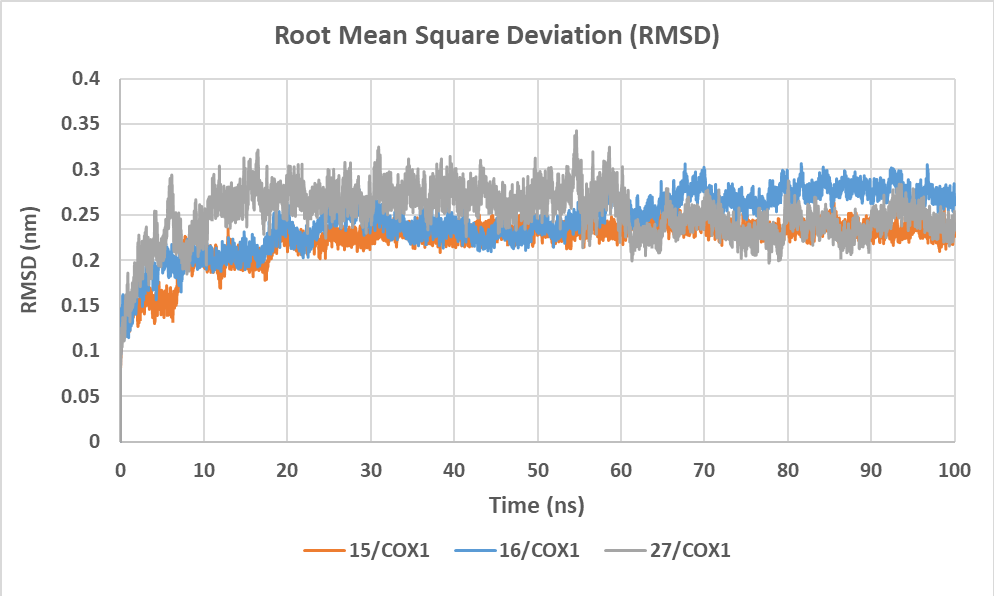

Figure S18. RMSD graph for the backbone atoms of **15**/COX-1 (orange), **16**/COX-1 (blue), and **27**/COX-1 (grey) structures from their initial reference frame backbone during 100 ns MD simulations

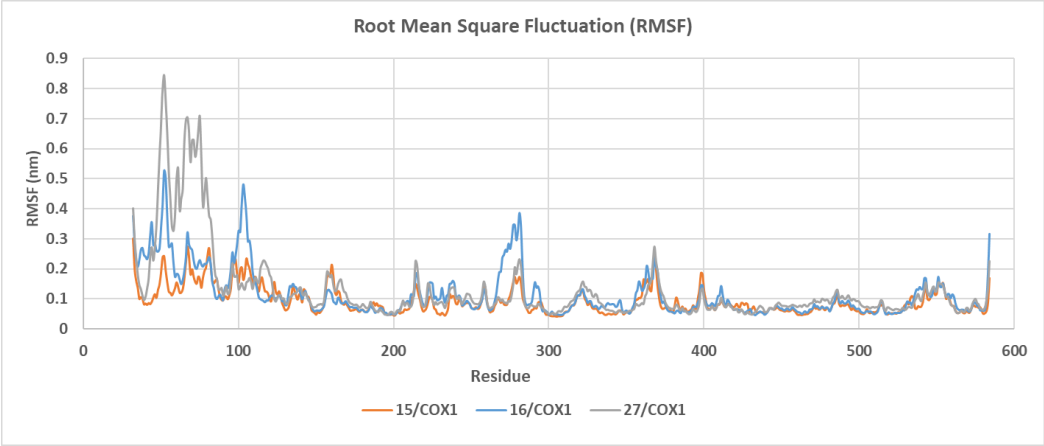

Figure S19. RMSF graph for the residues of **15**/COX-1 (orange), **16**/COX-1 (blue), and **27**/COX-1 (grey) structures during 100 ns MD simulation

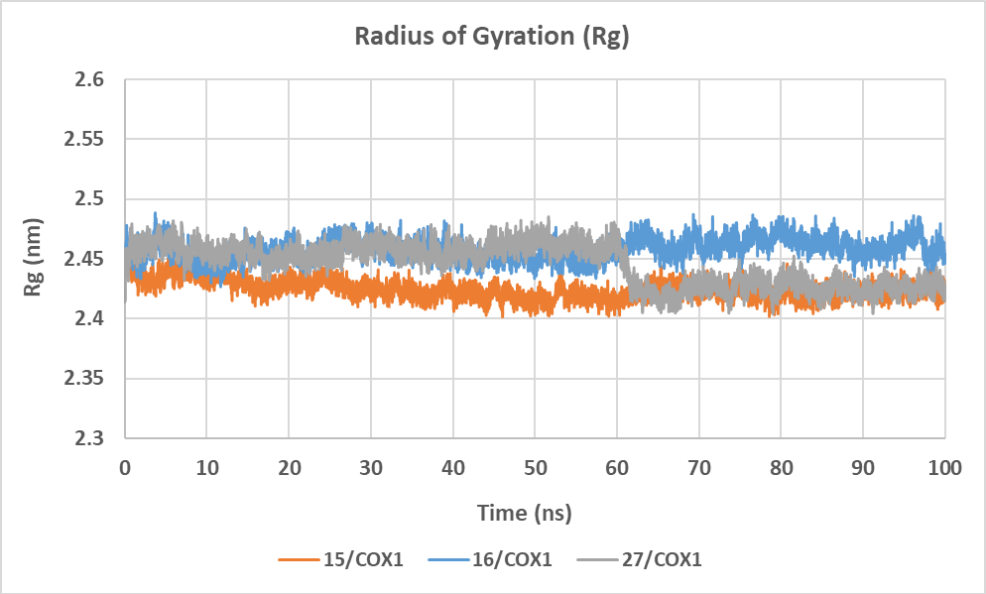

Figure S20. Radius of gyration (Rg) graph for **15**/COX-1 (orange), **16**/COX-1 (blue), and **27**/COX-1 (grey) structures during 100 ns MD simulation

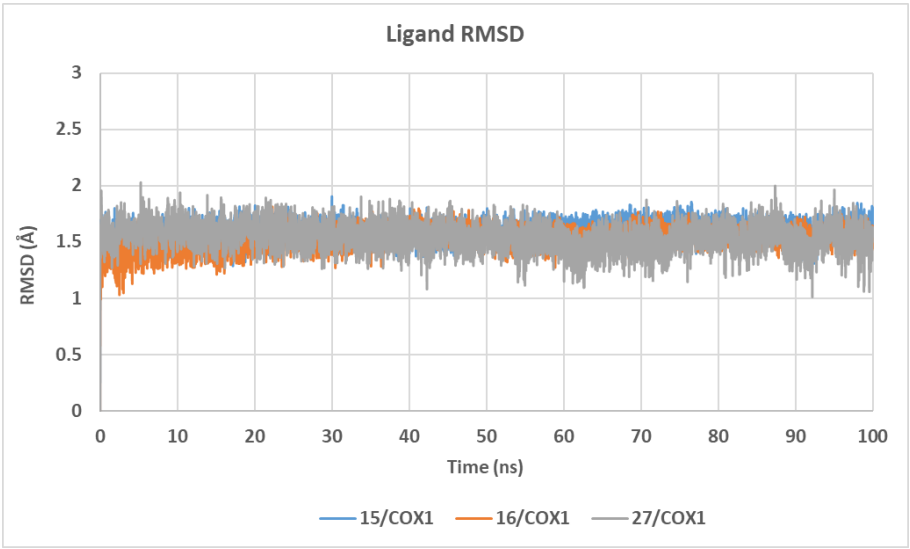

Figure S21. RMSD graph of compounds **15** (orange), **16** (blue), and **27** (grey) atoms from their initial pose in COX-1 structures during 100 ns MD simulation.

5.2 Dominant binding patterns of the target compounds 16 and 27 during the 100 ns MD simulations in COX-1 and COX-2

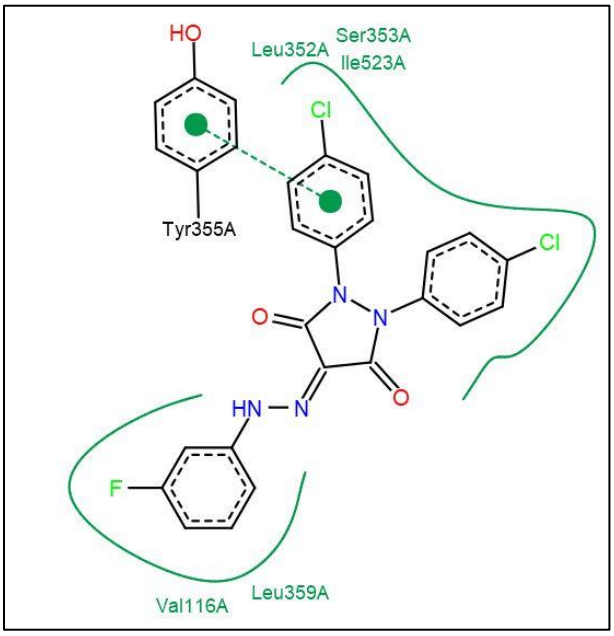

(A)

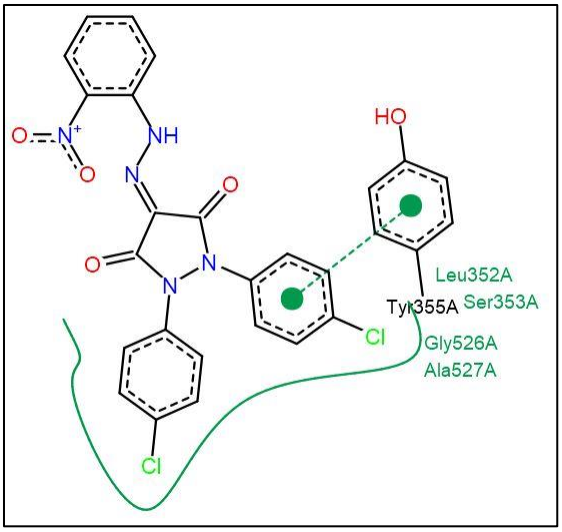

(B)

Figure S22. 2D diagram showing (A) compound **16** and (B) compound **27** dominant binding patterns in the active site of COX-1

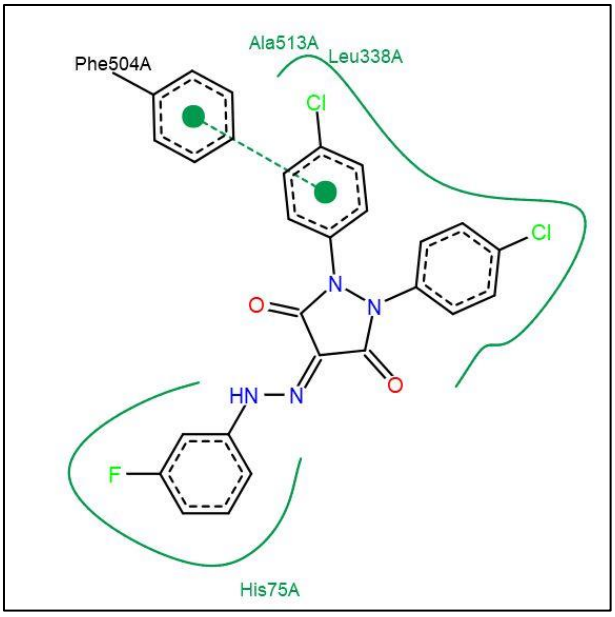

(A)

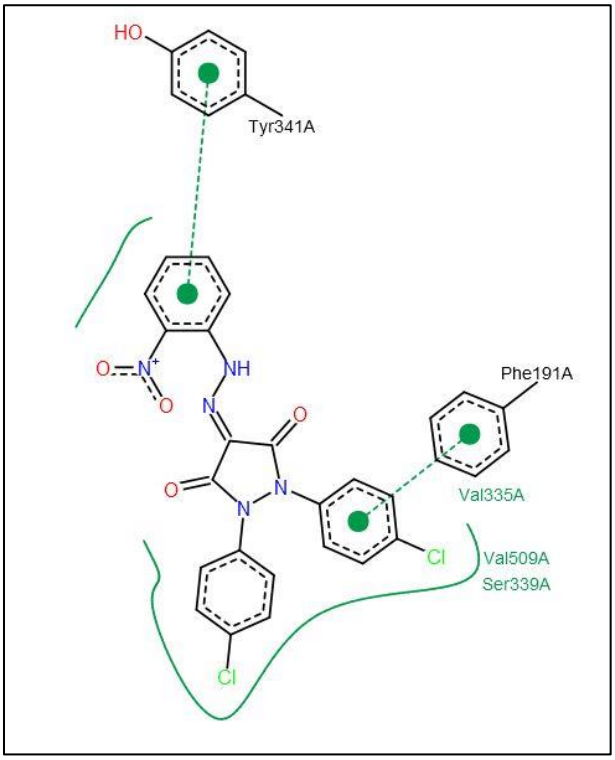

(B)

Figure S23. 2D diagram showing (A) compound **16** and (B) compound **27** dominant binding patterns in the active site of COX-2

6. Figures S24–S25

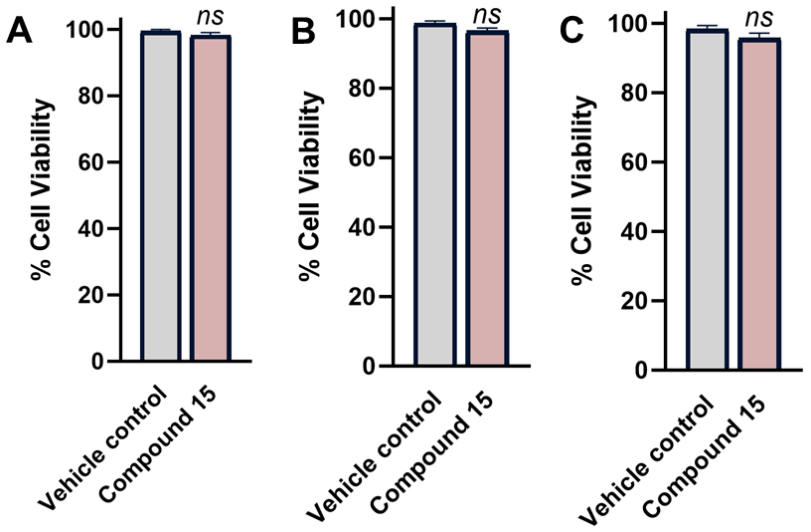

Figure S24. Cell viability as assessed by PrestoBlue of NHA **(A)**, hBMECs **(B)**, and HepG2 **(C)** upon incubation with a single dose of 50 μM of compound **15** after 72 h incubation. (*ns*) denotes nonsignificant relative to vehicle control. Error bars represent standard deviation (n = 3).

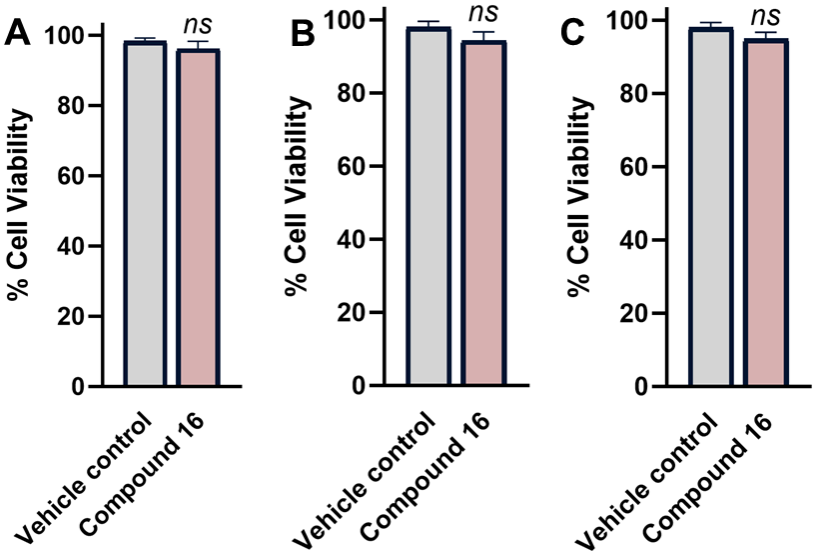

Figure S25. Cell viability as assessed by PrestoBlue of NHA **(A)**, hBMECs **(B)**, and HepG2 **(C)** upon incubation with a single dose of 50 μM of compound **16** after 72 h incubation. (*ns*) denotes nonsignificant relative to vehicle control. Error bars represent standard deviation (n = 3).

References

[1] E.M. Gedawy, A.E. Kassab, A.M.E. Kerdawy, Design, synthesis and biological evaluation of novel pyrazole sulfonamide derivatives as dual COX-2/5-LOX inhibitors, Eur.J. Med. Chem., 189 (2020) 112066.
[2] G. Cingolani, A. Panella, M.G. Perrone, P. Vitale, G.D. Mauro, C.G. Fortuna, R.S. Armen, S. Ferorelli, W.L. Smith, A. Scilimati, Structural basis for selective inhibition of Cyclooxygenase-1 (COX-1) by diarylisoxazoles mofezolac and 3-(5-chlorofuran-2-yl)-5-methyl-4-phenylisoxazole (P6), Eur J Med Chem, 138 (2017) 661-668.
[3] J.L. Wang, D. Limburg, M.J. Graneto, J. Springer, J.R. Hamper, S. Liao, J.L. Pawlitz, R.G. Kurumbail, T. Maziasz, J.J. Talley, J.R. Kiefer, J. Carter, The novel benzopyran class of selective cyclooxygenase-2 inhibitors. Part 2: the second clinical candidate having a shorter and favorable human half-life., Bioorg. Med. Chem. Lett., 20 (2010) 7159-7163.
[4] RCSB Protein Data Bank, https://www.rcsb.org/ (accessed September 7, 2025).
[5] Discovery Studio visualized 2017R2, in, Dassault Systèmes BIOVIA, San Diego, 2016, in.
[6] B.P. Kelley, S.P. Brown, G.L. Warren, S.W. Muchmore, POSIT: Flexible Shape-Guided Docking For Pose Prediction, J Chem Inf Model., 55 (2015) 1771-1780.
[7] M. McGann, FRED pose prediction and virtual screening accuracy, J. Chem. Inf. Model. , 51 (2011) 578-596.
[8] M. McGann, FRED and HYBRID docking performance on standardized datasets, J Comput Aided Mol Des, 26 (2012) 897-906.
[9] OEDOCKING 3.2.0.2, in, OpenEye Scientific Software, Santa Fe, NM, 2018, in.
[10] P.C.D. Hawkins, A.G. Skillman, G.L. Warren, B.A. Ellingson, M.T. Stahl, Conformer Generation with OMEGA: Algorithm and Validation Using High Quality Structures from the Protein Databank and Cambridge Structural Database, J. Chem. Inf. Model., 50 (2010) 572-584.
[11] P.C.D. Hawkins, A.G. Skillman, G.L. Warren, B.A. Ellingson, M.T. Stahl, OMEGA 3.0.0.1, in, OpenEye Scientific Software, Santa Fe, NM, (2018).
[12] K. Stierand, M. Rarey, Drawing the PDB: Protein-Ligand Complexes in Two Dimensions, ACS Med Chem Lett., 1 (2010) 540-545.
[13] K. Stierand, M. Rarey, From modeling to medicinal chemistry: automatic generation of two-dimensional complex diagrams, ChemMedChem., 2 (2007) 853-860.
[14] K. Stierand, P.C. Maaß, M. Rarey, Molecular complexes at a glance: automated generation of two-dimensional complex diagrams, Bioinformatics 22 (2006) 1710-1716.
[15] K. Stierand, M. Rarey, PoseView, in, BioSolveIT GmbH, St. Augustin - Germany.
[16] E.F. Pettersen, T.D. Goddard, C.C. Huang, G.S. Couch, D.M. Greenblatt, E.C. Meng, T.E. Ferrin, UCSF Chimera—A visualization system for exploratory research and analysis, J Comput Chem, 25 (2004) 1605-1612.
[17] M.J. Abraham, T. Murtola, R. Schulz, S. Páll, J.C. Smith, B. Hess, E. Lindahl, GROMACS: High performance molecular simulations through multi-level parallelism from laptops to supercomputers, SoftwareX, 1-2 (2015) 19-25.
[18] K. Lindorff-Larsen, S. Piana, K. Palmo, P. Maragakis, J.L. Klepeis, R.O. Dror, D.E. Shaw, Improved side-chain torsion potentials for the Amber ff99SB protein force field, Proteins, 78 (2010) 1950-1958.

[19] J. Wang, R.M. Wolf, J.W. Caldwell, P.A. Kollman, D.A. Case, Development and testing of a general amber force field, J Comput Chem, 25 (2004) 1157-1174.
[20] J. Wang, W. Wang, P.A. Kollman, D.A. Case, Automatic atom type and bond type perception in molecular mechanical calculations, J Mol Graph Model, 25 (2006) 247-260.
[21] A.W. Sousa da Silva, W.F. Vranken, ACPYPE - AnteChamber PYthon Parser interfacE, BMC Res Notes, 5 (2012) 367.
[22] G. Bussi, D. Donadio, M. Parrinello, Canonical sampling through velocity rescaling, J Chem Phys, 126 (2007) 014101.
[23] H.J.C. Berendsen, J.P.M. Postma, W.F. van Gunsteren, A. DiNola, J.R. Haak, Molecular dynamics with coupling to an external bath, J Chem Phys, 81 (1984) 3684-3690.
[24] B. Hess, H. Bekker, H. Berendsen, J. Fraaije, LINCS: A Linear Constraint Solver for molecular simulations, J Comput Chem, 18 (1997) 14631472.
[25] M. Parrinello, A. Rahman, Polymorphic transitions in single crystals: A new molecular dynamics method, J Appl Phys, 52 (1981) 7182-7190.
[26] T. Darden, D. York, L. Pedersen, Particle mesh Ewald: An N·log(N) method for Ewald sums in large systems, J Chem Phys, 98 (1993) 10089-10092.
[27] K.L. Damm, H.A. Carlson, Gaussian-weighted RMSD superposition of proteins: a structural comparison for flexible proteins and predicted protein structures, Biophysical journal, 90 (2006) 4558-4573.
[28] V.N. Maiorov, G.M. Crippen, Significance of Root-Mean-Square Deviation in Comparing Three-dimensional Structures of Globular Proteins, J Mol Biol, 235 (1994) 625-634.
[29] E. Fuglebakk, J. Echave, N. Reuter, Measuring and comparing structural fluctuation patterns in large protein datasets, Bioinformatics, 28 (2012) 2431-2440.
[30] M.Y. Lobanov, N.S. Bogatyreva, O.V. Galzitskaya, Radius of gyration as an indicator of protein structure compactness, Mol Biol, 42 (2008) 623-628.